# GENERATION OF ANNUAL PERIOD ROSSBY WAVES IN THE
# SOUTH ATLANTIC OCEAN BY THE WIND STRESS CURL

By

## CHRISTOPHER JAMES CHARLES REASON

B.Sc(Hons).,University of Cape Town, 1982

M.Phil.,The City University,London, 1985

A THESIS SUBMITTED IN PARTIAL FULFILLMENT OF

THE REQUIREMENTS FOR THE DEGREE OF

MASTER OF SCIENCE

in

## THE FACULTY OF GRADUATE STUDIES

Department of Oceanography

We accept this thesis as conforming

to the required standard

## THE UNIVERSITY OF BRITISH COLUMBIA

July 1986

In presenting this thesis in partial fulfilment of the requirements for an advanced degree at the University of British Columbia, I agree that the Library shall make it freely available for reference and study. I further agree that permission for extensive copying of this thesis for scholarly purposes may be granted by the head of my department or by his or her representatives. It is understood that copying or publication of this thesis for financial gain shall not be allowed without my written permission.

Department of ___Oceanography___

The University of British Columbia
1956 Main Mall
Vancouver, Canada
V6T 1Y3

Date ___28/8/86___

# Abstract

A theoretical study is presented of generation of first mode annual period baroclinic Rossby waves by the observed wind stress curl in the South Atlantic and South West Indian Oceans. The forcing wind field for the area 15 S to 51 S, 45 W to 41 E was obtained from an harmonic analysis at the annual period of the monthly mean wind stress curl values derived from Hellerman and Rosenstein's 1983 data.

The annual harmonic of the wind stress curl was then used to drive a linear, reduced gravity model of the South Atlantic and South West Indian Oceans bounded by the latitudes 15 S and 51 S and by longitudes 46 W and 50 E. Boundary geometries and oceans are represented to 1.0 and 0.2 degree accuracy, respectively, by a finite difference grid in spherical polar co-ordinates. Successive over-relaxation and a leap frog time differencing scheme are used to solve the two dimensional Rossby wave equation which includes relative vorticity and a Rossby radius that varies with latitude. By assuming quasi-geostrophy, the steady state model response is restricted to first mode baroclinic Rossby waves.

In the model South Atlantic Ocean, the response consists of long Rossby waves which generally propagate south westwards across the ocean and which exhibit refraction of wave energy towards the equator as in the theory of Schopf et al (1981). Short Rossby waves with eastward energy propagation are generated in the small area of the Indian Ocean included in the model domain. However, since the model grid has a resolution of approximately 22 km these waves may not be sufficiently accurately represented in the study. Medium to long waves generated to the south east of Africa may reflect their energy off this landmass into the Indian Ocean.

Slowness curve theory and wavenumber computations along wave rays in the South Atlantic are applied to match the model wave trains with probable sources. It is found that wind stress curl maxima off the Namibian coast near 25 S,10 E, near the Agulhas Plateau at 38 S,25 E and in the South Atlantic Ocean interior near 38 S,10 W are the most efficient wave generators. The results of the study are generally consistent with earlier theoretical studies of the North Pacific by White and Saur (1981) and by Cummins et al (1986) and

of the North Atlantic by Krauss and Wuebber (1982).

# Contents

# List of Figures

history of the slowness circles is from top to bottom.

Figure 7b. Slowness curve showing refraction of wave energy starting near 33 S,20 W. Time history of the slowness circles is from top to bottom.

Figure 7c. Slowness curve showing reflection and subsequent refraction of wave energy near 33 S,30 E. Time history of the slowness circles is from top to bottom.

Figure 7d. Slowness curve showing refraction of wave energy near 41 S, 30 E. Time history of the slowness circles is from top to bottom.

Figure 7e. Slowness curve showing direction of wave energy propagation near 30 S,35 E.

Figure 7f. Slowness curve showing reflection of wave energy off an idealised wall.

Figure 8a. Longitude-time plot of the thermocline height field along 40 S.

Figure 8b. Longitude-time plot of the thermocline height field along 31 S.

Figure 8c. Longitude-time plot of the thermocline height field along 25 S.

Figure 8d. Longitude-time plot of the thermocline height field along 35 S.

Figure 8e. Longitude-time plot of the thermocline height field along 42 S.

Figure 8f. Longitude-time plot of the thermocline height field along 45 S.

Figure 9. Wavenumber vectors computed at points along wave rays near 20 S, 32 S, 35 S and 40 S. Units of wavenumber magnitude are $10^{-5}$ $m^{-1}$.

Figure 10. Root mean square geostrophic velocities of magnitude 5 $cm$ $s^{-1}$ or less associated with the Rossby wave field.

Figure 11. Root mean square geostrophic velocities of magnitude 5 $cm$ $s^{-1}$ or more associated with the Rossby wave field.

Figure 12. Instantaneous geostrophic velocities associated with the thermocline height field shown in Figure 4a. Scaling : a 1 cm long vector corresponds to a velocity of 4.6 $cm$ $s^{-1}$.

Figure 13. Slowness curve representation of the dispersion relation for free Rossby waves.

Figure 14. The form of the damping layers imposed along the northern, western and eastern boundaries of the model domain.

## Acknowledgements

# 1.Introduction

The generation of Rossby waves at the eastern boundary of a mid- latitude ocean by a seasonally varying wind stress curl has been the subject of several recent studies, (White and Saur, 1981; Krauss and Wuebber, 1982 and Cummins et al, 1986). In contrast to the northern hemisphere focus of these papers, this study is the first to consider Rossby wave generation in the South Atlantic Ocean. The approach adopted for this problem is to apply the model of Cummins et al (1986) to the South Atlantic region. As these authors show, their model is able to explain the westward propagation of annual period Rossby waves observed by Kang and Magaard (1980) and Price and Magaard (1983) in the North Pacific.

Although the South East Atlantic and the Benguela current region have been of interest to oceanographers in the past because of the pronounced seasonal upwelling that occurs there, no work to date has been done on the possibility of Rossby wave generation in this area. Motivation for considering the central South Atlantic as an area for Rossby wave propagation follows from the fact that like the central North Pacific and North Atlantic Oceans it is a relatively quiet ocean in terms of eddy activity and mesoscale variability (Cheney et al, 1983). In addition there is the pronounced seasonal wind stress curl that is necessary for the generation of annual period Rossby waves. South of 40 S in the South Atlantic as well as further north near the southern coast of South Africa, this is not the case. Numerous studies report eddies, meanders and frontal activity in this area (see for example Duncan, 1968; van Foreest et al, 1984; Lutjeharms and Valentine, 1984; and Shannon, 1985). Apart from these regions, it can be expected that the central South Atlantic will be characterised by similar quasigeostrophic dynamic balances as occur in the central North Pacific (Thomson, 1986). Since Rossby waves have been observed in this ocean it is likely that these waves may also exist in the central South Atlantic Ocean.

In order to represent the central South Atlantic Ocean effectively and to exclude the possibility of edge effects the model domain is chosen to extend from 15 S to 51 S and from 46 W to 50 E. Note that as a result of this size of domain there is also scope for

1

generation of waves in regions other than along the south western coast of Africa. In particular, the ocean to the south of the tip of Africa (Cape Agulhas) where the Agulhas, Antartic Circumpolar and Benguela currents approach each other and which has always been noted by seamen for its stormy conditions, is a likely area for wind generated Rossby waves. Also, the possible existence of localised maxima in the mid ocean wind stress curl may give rise to Rossby waves (e.g. see Haidvogel and Rhines, 1983).

There are other oceanic processes besides seasonal wind forcing at the sea surface which may act as vorticity sources and so produce baroclinic Rossby waves. Killworth (1979) cites storms, mean flow instabilities of western boundary currents and of mid-ocean currents, scattering from flows over topography and around irregular coastlines, and radiation from coastally trapped waves. The last mentioned mechanism has been considered in a paper by White and Saur (1983) in which short term climatic variability of sea level fluctuations associated with poleward propagating coastally trapped Kelvin waves act as a source of interannual westward travelling Rossby waves which emanate from the Pacific coast of Central America between 20 N and 30 N. Further north, they find the wind stress curl to be the dominant source of the waves.

Another possible generating mechanism is the fluctuation in the surface buoyancy flux. Magaard (1977) considered this to be a likely source of the very long, low frequency baroclinic waves observed by Emery and Magaard (1976) in the Eastern Pacific. In addition to buoyancy forcing, Magaard also considered fluctuating wind stress and atmospheric pressure at the sea surface as sources but concluded that the pressure mechanism is unlikely to be important. In a recent study, McCreary et al (1986) drive a model of an eastern boundary current region with both a seasonal wind stress curl and seasonal thermohaline forcing. However, they find that Rossby waves are generated solely by the wind field. The region of application of their model is the Leeuwin Current area off the west coast of Australia and it is found that it is the thermohaline forcing which drives this current.

Oscillations in boundary currents on the seasonal time scale have been shown to be a potential source of Rossby waves (Mysak, 1983). This mechanism could be of potential

significance in the South Atlantic and South Indian Oceans due to observed meanders and fluctuations in both the Agulhas current proper and in its retroflection point (defined as the point south of Africa where the most of the Agulhas Current turns back into the Indian Ocean instead of flowing around the continent into the South Atlantic - its position is centred around 40 S,20 E (Harris et al, 1978)). Note that there has been substantial theoretical interest in modelling the Agulhas retroflection (e.g. see de Ruijter, 1982; Lutjeharms and van Ballegooyen, 1984; Ou and de Ruijter, 1985; de Ruijter and Boudra, 1985; Boudra and de Ruijter, 1986). However, since these models all employ steady dynamics the possible generation of Rossby waves by the long period fluctuations in the retroflection point is ignored. In addition, there is transport of water masses in the neighbourhood of the retroflection from the Indian into the Atlantic Ocean (Gordon, 1985). Also mesoscale eddies have been observed to shed off from the region (Harris et al, 1978; Lutjeharms, 1981; Gruendlingh, 1983; Olson and Evans, 1986). All these processes could play a role in Rossby wave dynamics. It should be emphasised though, that these transients in the Agulhas current system would need to be at the annual period to produce any Rossby waves since the critical latitude for waves at shorter periods is equatorward of this region (e.g. a wave of period 6 months has a critical latitude of about 30 S). However, recent satellite studies of the Southern Benguela current system (van Foreest et al 1984; Shannon, 1985) have found evidence of eddies and stationary frontal features between 20 S and 35 S. Since this is somewhat nearer the equator than the Agulhas Retroflection region, such features could interact with or produce Rossby waves, providing their time scales were of the order of 6 months or more.

Finally, as LeBlond and Mysak (1978) mention, penetrative convection (i.e. the sinking of cold water) and internal wave stresses could also generate Rossby waves under certain conditions.

In summary, there are a number of ways in which Rossby waves could arise in the ocean. However, in this thesis, attention is restricted to generation of Rossby waves by the seasonally varying wind stress curl that is observed to exist in the South Atlantic and

South West Indian Oceans (see Section 3 for details). The seasonally varying wind stress curl mechanism has been shown by White and Saur (1981) and Cummins et al (1986) to be an efficient generator of Rossby waves in the North Pacific Ocean. In addition, Thomson (1986) has found that this ocean has similar dynamic balances and levels of variability as the central South Atlantic Ocean.

As discussed in Cummins et al (1986), the model makes use of the two dimensional (dispersive) Rossby wave equation cast in spherical polar coordinates. This allows both refractive and dispersive effects to be treated. It also includes a realistic representation of the boundary geometry which in this study is the 1000m isobath off the coast of Southern Africa.

Use of the observed rather than an idealised wind forcing represents a significant step forward from earlier analytic models. For example, White and Saur (1981) assumed the coastal wind stress curl to have constant amplitude whereas Krauss and Wuebber (1982) approximated the longshore winds off Western Europe and North Africa by the function $cos\frac{2\pi y}{\lambda}$ where y is the latitude and $\lambda$, the wavelength, is of the order of 6000km. Another feature of the model is the solid boundary on all sides of the ocean with appropriate damping layers to prevent reflection of outward propagating wave energy back into the domain. Note that the southern boundary of 51 S is nearer the pole than the 47.2 S critical latitude for Rossby waves at the annual period so no damping is needed there. Also, the South American coast which impinges on the western boundary in the top left hand corner of the model domain is absorbed into the sponge layer as are the rest of the western and equatorial boundaries.

An outline of the contents of this thesis is as follows. Section 2 gives a brief description of the governing equations for the model together with the underlying assumptions and methods of solution. Further details on the governing equations and the dispersion relation can be found in the Appendix. A discussion of the wind stress curl forcing for the model is presented in Section 3. The model results are discussed in Section 4. A detailed analysis of the results is given in Section 5. Finally, Section 6 presents the conclusions arising from

the study and some suggestions for future work.

## 2.Governing Equations

The governing equations used in the model are the linearised reduced gravity equations which when written in spherical polar coordinates are

$$\frac{\partial u}{\partial t} - fv + \frac{g'}{a\cos\theta}\frac{\partial h}{\partial \lambda} = \frac{\tau^\lambda}{\rho_o H_o} - r_o u, \tag{2.1a}$$

$$\frac{\partial v}{\partial t} + fu + \frac{g'}{a}\frac{\partial h}{\partial \theta} = \frac{\tau^\theta}{\rho_o H_o} - r_o v, \tag{2.1b}$$

$$\frac{\partial h}{\partial t} + \frac{H_o}{a\cos\theta}\left(\frac{\partial(v\cos\theta)}{\partial \theta} + \frac{\partial u}{\partial \lambda}\right) = -r_o h, \tag{2.1c}$$

where $\lambda$ and $\theta$ are the zonal and meridional spherical coordinates with associated velocities u and v respectively, h is the interfacial displacement (positive downwards), $\tau^\lambda$ and $\tau^\theta$ are the eastward and northward wind stress components, f is the Coriolis parameter, a is the earth's radius, $g'$ is the reduced gravity and $\rho_o$ and $H_o$ are the density and unperturbed thickness of the upper layer of the ocean. Note that the friction coefficient $r_o$ acts as a Rayleigh damping in the momentum equations (2.1a,2.1b) while in (2.1c) it has the form of a Newtonian cooling.

In order to rewrite the above three equations in terms of a single vorticity equation for the thermocline displacement h, the quasigeostrophic assumption is made. Use of this assumption is based on the facts that away from intense western boundary current regions the ocean is always close to geostrophic equilibrium and that when this quasi-equilibrium is disturbed the ocean adjusts to a new near equilibrium state. There are two time scales at which this adjustment occurs, a faster scale of the order of 1/f characteristic of inertia-gravity waves and a slow scale of months to years characteristic of planetary or Rossby waves. Details of how the quasi-geostrophic assumption is actually imposed on the dynamics can be found in any standard text, for example Gill (1982) or Pedlosky (1979), but in essence it involves expanding the governing equations to first order in the Rossby number U/fL, which is assumed to be small. A major advantage of assuming quasi-geostrophy is that it filters out Kelvin and inertia-gravity waves from the model which means that the possibility of Rossby waves being generated at the eastern boundary

by a poleward propagating Kelvin wave, as in the model of White and Saur (1983), need not be considered. As a result of the quasi-geostrophic approximation we have the vorticity equation

$$(\frac{\partial}{\partial t} + r_o)(\nabla^2 - R^{-2})h + \frac{\beta}{a\cos\theta}\frac{\partial h}{\partial \lambda} = \frac{1}{\rho_o f R^2} curl_z \tau, \qquad (2.2)$$

$R(\theta) = \sqrt{g'H_o}/f$ is the internal Rossby radius, which in the model is allowed to vary with latitude, and $\beta = 2\Omega\cos\theta/a$ is the gradient of planetary vorticity ($\Omega$ and a being the earth's angular velocity and radius respectively). The operator $\nabla^2$ is the horizontal Laplacian which when written in spherical coordinates takes the form

$$\nabla^2 = \frac{1}{a^2\cos\theta}(\frac{1}{\cos\theta}\frac{\partial^2}{\partial\lambda^2} + \frac{\partial}{\partial\theta}(\cos\theta\frac{\partial}{\partial\theta}))$$

The model equations are based on the following assumptions :

1. The ocean is comprised of two homogeneous and incompressible layers which are non-mixing and are separated by a thin thermocline.

2. Wind stress forcing acts as a body force in the upper layer only.

3. Horizontal pressure gradients in the lower layer vanish.

4. Viscous effects are represented simply by the $r_o$ terms.

5. No variations in the bottom topography (e.g. the possible effects of the Walvis Ridge, which extends from the mid-Atlantic Ridge to the Namibian coast, are ignored).

6. Non linear effects (e.g. interaction with the Benguela and South Equatorial Currents or with eddies shed by the Agulhas retroflection) are ignored.

7. $H_o$, the depth of the unperturbed upper layer, is assumed constant.

8. There is no barotropic mode.

Motivation for considering the first baroclinic mode alone (i.e. a reduced gravity model) lies in the fact that the effect of wind stress in areas with a strong thermocline is to excite this mode preferentially (McCreary, 1976; Moore and Philander, 1976). Also, Krauss and Wuebber (1982) found that far from the coast their model response was dominated by the first baroclinic mode.

Because the governing equations are linear, the response of the model to forcing at any given frequency can be described solely in terms of that frequency. Hence the wind stress curl forcing used in the model takes the form of the harmonic

$$curl_z \underline{\tau} = A(\lambda, \theta)cos(\omega t + \phi(\lambda, \theta))$$

where $A(\lambda, \theta)$ and $\phi(\lambda, \theta)$ are the amplitude and phase respectively and have been computed by the harmonic analysis described in Section 3. For reasons given in that section the frequency chosen to force the model corresponds to the annual period.

Based on the experience gained from running the model for the North Pacific region (Cummins et al, 1986), boundary conditions have been chosen which prevent the wave energy from being reflected back into the model domain and so leading to unphysical results. As described in Cummins et al (1986), the procedure is to treat the three open ocean boundaries as well as the land as solid walls with no normal flow, i.e. $h = 0$ there. By imposing damping layers at all open ocean boundaries, excepting that along 51 S, reflection of wave energy is avoided. The reason for not putting any damping on the southern boundary is that it lies poleward of the critical latitude for annual period Rossby waves and so any wave energy approaching this latitude will be refracted back into the domain by the model equations. This process would occur in the real ocean. On the other ocean boundaries the damping attenuates incoming Rossby wave energy via the Rayleigh friction/ Newtonian cooling coefficient which increases from zero in the open ocean to a maximum at the solid wall. Details of how the appropriate values of the coefficient are arrived at can be found in the Appendix. It is crucial that the attenuation effect of the damping is correct as otherwise reflection of energy and possible concentrations of energy in the corners of the model domain may occur. The reason for not choosing the seemingly more physical radiation condition (e.g. those suggested by Camerlengo and O'Brien (1980) and Raymond and Kuo (1984)) is that these conditions have been developed for waves which have their phase and group velocities in the same direction - a property which does not generally apply to Rossby waves.

On the other hand, the termination of the African continent in mid-ocean allows possible reflection of any Rossby waves generated to the south or east of this boundary, i.e. in the south west Indian and Southern Oceans. It is quite feasible that such reflection might occur in the real ocean and so no damping layer is imposed along the African continent. Although the South American continent does in fact impinge on the model domain in the top left hand corner, no distinction is made between it and the adjacent open ocean boundaries. In other words this small area of land is ignored and the grid points corresponding to its location are simply treated as part of the damping layer.

Figure 1 is the finite difference representation of the South Atlantic and South Indian Oceans used as the model domain. The southern African coastline is resolved by the model grid to within one degree of latitude and longitude. Superimposed on the diagram as hatched regions are the damping layers described above.

The values of the parameters used in the model are as follows :

$$g' = 1.5 \times 10^{-2} m \ s^{-2}$$

$$H_o = 500m$$

$$\rho_o = 1025kg \ m^{-3}$$

$$\omega = 2\pi/1year \ rad \ s^{-1}$$

$$\Omega = 7.29 \times 10^{-5} rad \ s^{-1}$$

$$a = 6371km$$

Note that the above values of $g'$ and $H_o$ are identical to those used by Cummins et al (1986) and Willmott (1985) for the North Pacific. The first mode Rossby radius of deformation resulting from these values of $g'$ and $H_o$ is the "best fit" to the zonal averages of the observed radii reported by Emery et al (1984). It is assumed that the above values of $g'$ and $H_o$, known to be appropriate for the North Pacific, are also reasonable for the South Atlantic and South Indian Oceans. Using the formulae for the Rossby radius and the critical latitude given in the Appendix it is found that the above values for the parameters

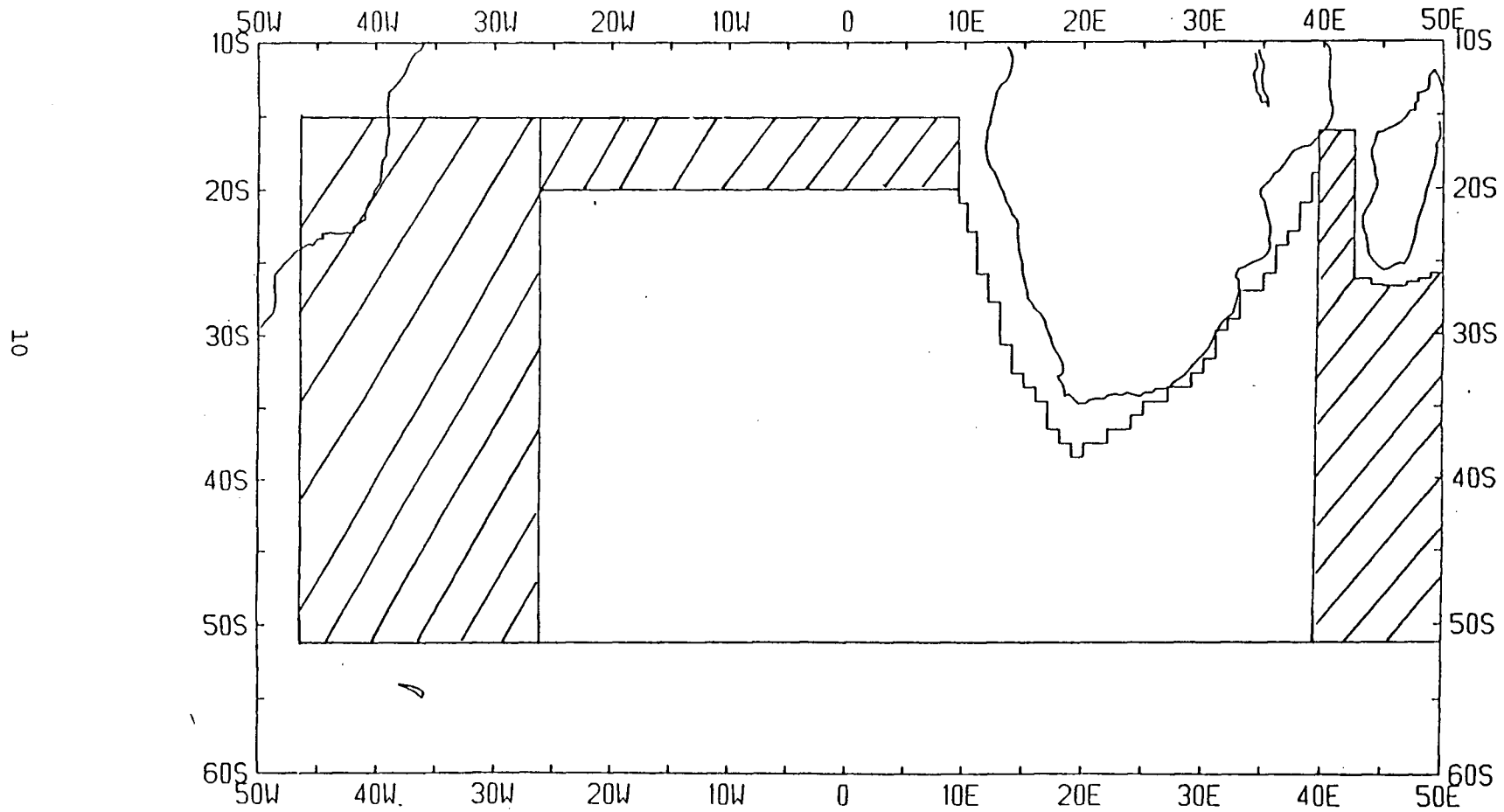# Model Domain and Damping Layers



Figure 1. The model domain with damping layers shown as hatched.

give a Rossby radius of 29.2 km at 40 S for example, whereas the critical latitude is 47. 2 S. As described above, the governing equations reduce to the single vorticity equation (2.2) which is to be solved for the model domain shown in Figure 1. It is represented by a finite difference grid of 481 longitude by 181 latitude points corresponding to a resolution of 0.2 degrees. As will be discussed in detail in Section 4, this satisfies the grid resolution condition for numerically modelling freely propagating Rossby waves derived by Wajsowicz (1986).

In order to solve equation (2.2) in as numerically efficient a way as possible it is rewritten as

$$(\partial_t + r_o)\varsigma + \left(\frac{2\Omega}{a^2}\right)\frac{\partial h}{\partial \lambda} = \frac{curl_z \tau}{\rho_o f R^2} \, , \tag{2.5}$$

where

$$\varsigma = (\nabla^2 - R^{-2})h, \tag{2.6}$$

and the definition of $\beta$ have been introduced.

Equation (2.5) is an advection equation for the vorticity field $\varsigma$ which can be solved using a leap-frog differencing scheme for the time variable and a centred differencing scheme for the spatial variable. The Helmholtz type equation (2.6) can be solved by a successive overrelaxation method in the Gauss-Seidel iteration to yield the height anomaly field h from the updated version of the vorticity $\varsigma$ obtained from (2.5). To start the model off from rest a forward difference time step was used. Each subsequent time step was 10 days whereas the spatial increment was 0.2 degrees for both the zonal and the meridional directions. Because the available observations of the wind forcing in the region of interest have a resolution of 2 degrees, a linear interpolation was used to represent the annual harmonic of the wind stress curl on the model grid. Within the damping layers the wind stress curl is set to zero.

## 3. Wind Stress Curl Forcing

Realistic wind stress curl forcing in the model was obtained from Hellerman's and Rosenstein's 1983 normal monthly windstress data. The windstress has been computed with 2 degree resolution from sea surface observations spanning a 106 year period from 1870-1976 using a bulk aerodynamic model for the drag coefficient. Specifically, the drag coefficient used by Hellerman and Rosenstein is a second order polynomial function of wind speed and stability similar to that used by Bunker (1976). In order to compute the vertical component of the wind stress curl, $curl_z \tau$, required for the forcing of the model, a finite difference approximation on a 2 by 2 degree grid as explained in Nelson (1977) was employed.

Since it is the low frequency variation in the wind stress curl that is particularly important for the generation of Rossby waves in the ocean, an harmonic analysis of the data at the annual period was performed to yield the amplitude and phase of the forcing.

The harmonic analysis involved a standard least squares fit (Foreman, 1977) of the monthly wind stress curl estimates to the sinusoidal form of the forcing used in the model. Figure 2a. shows the amplitude of the annual harmonic of the wind stress curl. Particularly large amplitudes are evident near the Namibian coast at about the 25 S latitude, in mid-ocean near 37 S,8 W and in a belt along the bottom of the model domain between 47 S and 51 S (the 'roaring forties'). Secondary maxima in the wind forcing are located to the south and east of the African coast at 38 S,25 E and near 25 S,35 E. Although the wind forcing maximum near the Namibian coast is expected to be the most important for Rossby wave generation, it is quite possible that localised wind maxima in the mid-ocean could produce Rossby waves (for example, Haidvogel and Rhines, 1983). On the other hand, the belt of maximum wind forcing in the far south of the domain is unlikely to be an important source of Rossby waves because this region is near the 47.2 S critical latitude for annual waves, (i.e. the latitude beyond which no Rossby waves can propagate at this frequency).

One further region for planetary wave generation in the South Atlantic which should be mentioned, is the interior tropical ocean immediately to the south of the equator. As
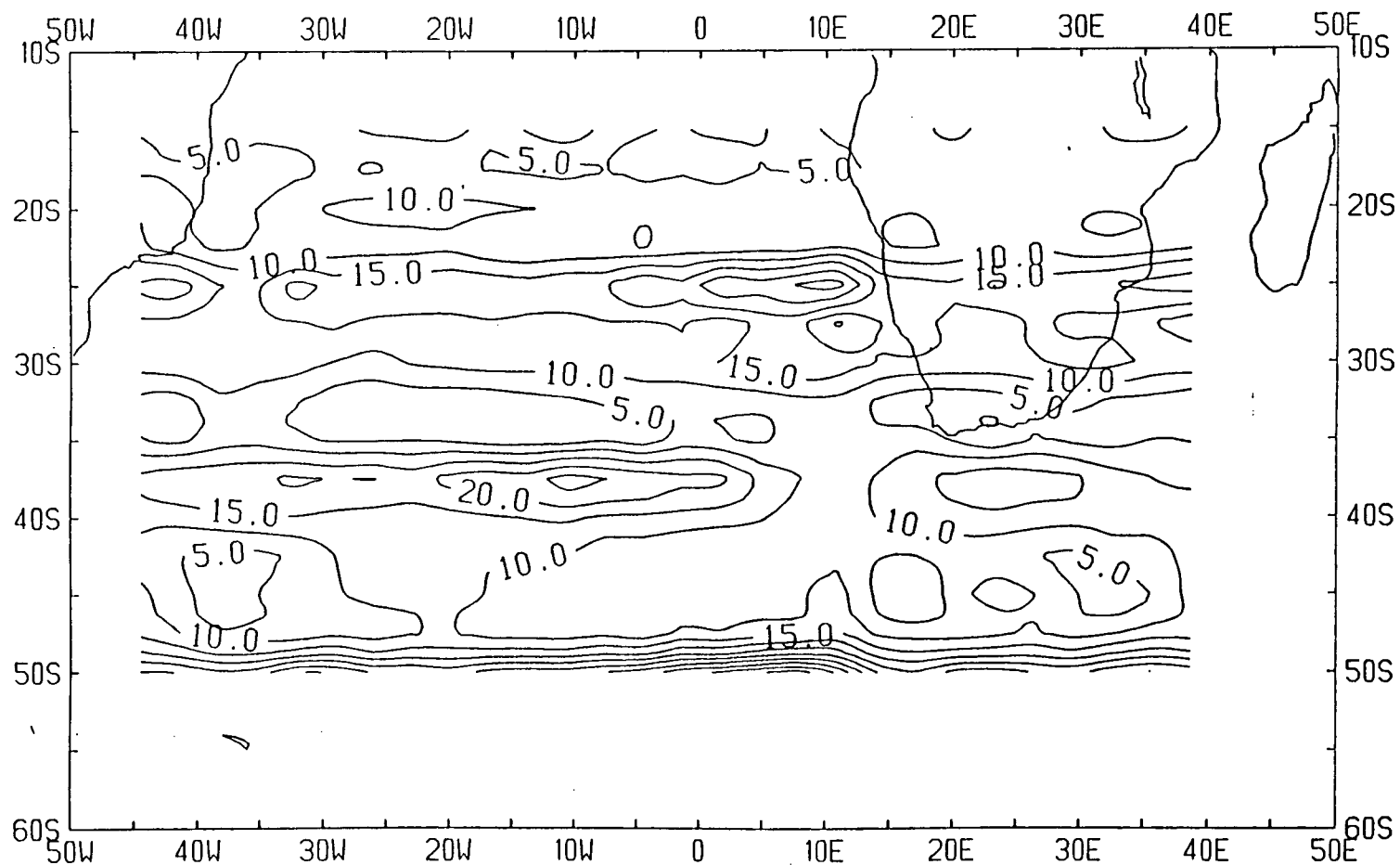
# WIND STRESS CURL



Figure 2a. Amplitude of the annual harmonic of the wind stress curl field over the area

15 S - 51 S,45 W - 41 E. Units are $10^{-9} dyne \ cm^{-3}$.

13

Figures 4 and 9 of Hellerman and Rosenstein's (1983) paper show, there is an annual variation in the wind field in this area. Also there are substantial seasonal seasonal variations in the thermocline in the tropical Atlantic (Cane and Sarachik, 1981). Despite its moderate strength in comparison to the wind at more southerly latitudes, it may still be of importance as a wave source because the Coriolis force balancing of any wind forcing disappears at the equator. However, any planetary waves generated there will be equatorially trapped due to this vanishing of the Coriolis force. According to McCreary (1976) the strongest interior tropical ocean response to wind anomalies is always confined to the equator.

The phase of the annual harmonic (Fig. 2b.) shows steep gradients in the vicinity of the South Atlantic anticyclone centred near 23 S,0 E and also along the 35 S to 37 S and 41 S to 43 S latitude bands. This latter zone indicates the transition between the subtropical and subpolar wind systems.

It should also be mentioned that the localised maxima in the winds near the African coast produce forced responses in the ocean in these areas and so in order that the no normal flow condition be satisfied at the boundary, free Rossby waves must be propagated out of the forcing region to the west. This is one way in which Rossby waves are generated by the wind. Waves can also be generated if the energy of the wind field is spread over a wide range of wavenumbers which include the resonance wave numbers of the Rossby waves themselves (Krauss and Wuebber, 1982). However, since the wind field in the South Atlantic Ocean is concentrated rather than evenly distributed this mechanism is not expected to be important.

Although detailed comparison is not possible, earlier studies by van Loon and Rogers (1984b) and Kamstra (1985) point to considerable variation in the wind field in the South Atlantic on a seasonal scale. The yearly wave in sea level pressure and zonal geostrophic wind has been analysed by van Loon and Rogers (1984b) from 12 years of daily synoptic maps. They find that the annual harmonic is strongest at 30 S near and over the three southern continents. This finding ties in with the observation by Hellerman and Rosenstein (1983) that the maximum wind stress curl shifts south from its July zonal position of 27

# Phase of annual harmonic (degrees)

|  | 50W | 40W | 30W | 20W | 10W | 0 | 10E | 20E | 30E | 40E | 50E |

```
        68  81  66  29  37  21  351 31  56  43  34  49  35  34  53  86  156 188 140 106 91  138
        142 133 40  298 356 323 310 325 155 101 99  165 115 140 156 127 183 190 160 156 174 172
        222 156 215 240 236 226 230 232 233 229 237 235 197 205 233 171 188 187 176 182 194 205
        210 193 178 212 214 215 232 225 232 241 255 267 242 225 231 122 208 208 216 205 264 236
        215 164 135 184 137 191 221 197 206 210 203 247 265 266 231 50  208 211 211 228 229 247
        229 242 244 249 253 262 265 257 240 244 253 256 255 251 248 258 247 244 243 241 232 237
        302 305 309 290 308 320 327 302 272 284 286 274 263 244 352 46  4   329 341 329 294 47
        24  29  31  38  37  42  34  29  24  36  43  57  53  47  56  64  51  41  34  33  33  39
        358 2   349 6   143 322 331 342 335 323 9   359 0   347 347 117 84  38  10  14  356 292
        338 321 325 344 273 51  55  85  344 343 340 340 348 334 338 260 68  5   24  35  1   275
        98  333 313 356 78  91  118 191 120 89  324 324 5   310 326 295 256 357 94  70  322 273
        121 122 112 122 124 136 139 130 128 123 129 123 127 140 139 152 149 132 125 118 107 137
        130 128 119 111 115 122 120 125 120 118 125 127 126 134 133 126 142 143 133 132 129 144
        179 157 73  323 4   348 330 338 210 122 112 217 150 180 256 147 219 223 194 184 203 203
        250 168 280 274 268 263 266 267 267 265 273 288 241 245 278 207 229 224 216 213 227 237
        243 237 210 248 247 246 265 263 257 263 280 293 280 265 270 92  246 245 241 244 315 264
        252 191 142 224 149 232 259 225 231 252 255 277 296 302 267 80  202 243 255 282 264 288
        260 276 278 281 292 294 298 291 272 274 288 292 285 282 277 292 280 278 281 276 266 271
        271 268 283 284 290 298 302 291 275 281 283 284 281 276 276 282 281 275 275 270 265 258
```

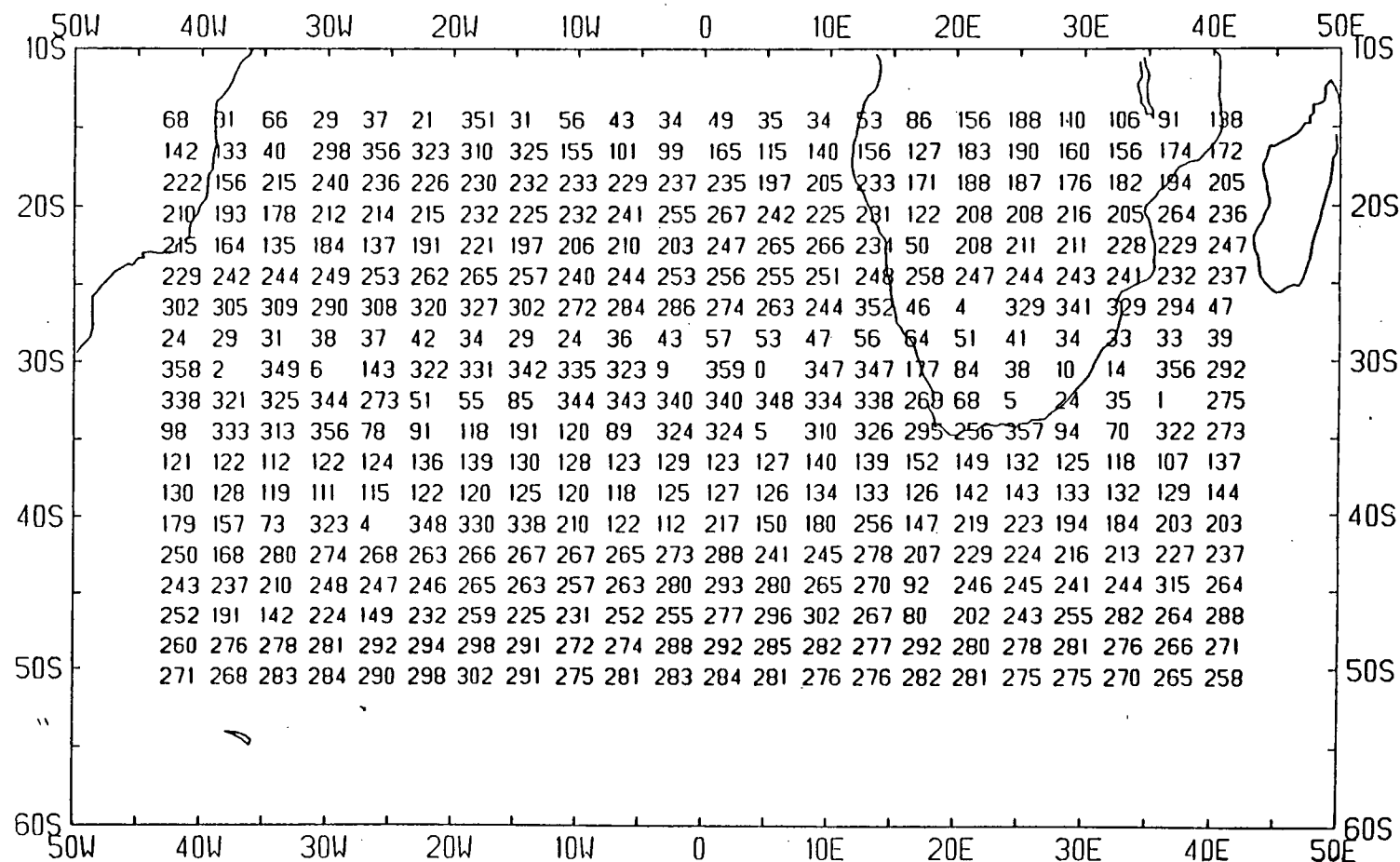|  | 50W | 40W | 30W | 20W | 10W | 0 | 10E | 20E | 30E | 40E | 50E |

Figure 2b. Phase of the annual harmonic of the wind stress curl field in degrees.

S to 34 S in January. At higher latitudes the yearly wave becomes second in importance to the half-yearly wave; the latter has peaks in amplitude between 45 S and 50 S and near 60 S (van Loon and Rogers, 1984a). However, the likelihood of the semi-annual harmonic in the wind field being important for Rossby wave generation is not great because the critical latitude for waves at this frequency is of the order of 30 S. On the other hand, the critical latitude of 47.2 S for the annual waves is well to the south of the peak in the yearly harmonic of the winds.

A useful synopsis of the wind stress field in the Southern Benguela current region, which is one of the most likely source areas for the Rossby waves, has been provided by Kamstra(1985). It is as follows. During the austral summer strong heating over the southern African subcontinent leads to low pressures there which contrast with the South Atlantic anticyclone situated some 2000km offshore. As a result there are pronounced pressure gradients which in turn lead to strong south easterly winds along the south and west coasts of southern Africa. In the southern winter, after the circumpolar low pressure belt and South Atlantic anticyclone have migrated towards the equator, one tends to find westerly to north westerly winds prevailing over the south western coastal area of South Africa (i.e. 32 S to 35 S) whereas north of this region the southerly winds, though generally weaker than those of summer, still prevail.

# 4. The Model Rossby Wave Field

In order to obtain a steady state Rossby wave response to the wind forcing, the model was integrated until all transients in the solution had died out and the resulting model behaviour consisted of a uniform sinusoidal oscillation about a zero mean at all points in the domain. Figure 3 shows the typical response at a representative point. The steady-state behaviour required some 42 years of integration time and the resulting Rossby wave field is plotted in Figure 4a. The solid lines in the plot are positive contours of the thermocline depth anomaly for Julian day 1 (January 1st) of the model year whereas the dashed lines are the negative displacements (i.e. towards the sea surface) of the thermocline. Figure 4b. is a contoured plot of the Rossby wave situation 90 days later, i.e. April 1st in the model year. Plots of the wave field for June 1st and September 1st are identical to Figures 4a. and b. respectively provided that the solid and dashed lines are interchanged. An indication of how the process of phase propagation of the Rossby wave field occurs is evident in Figure 4c. which is a plot of the thermocline distribution 40 days after that shown in Figure 4b.

From these plots it is clear that the Rossby wave field in much of the South Atlantic is dominated by long waves with a maximum amplitude of 24 m. Both the phase and the energy of the waves propagate westwards across the ocean. As an example consider the wave crest to the south west of Cape Agulhas at 41.5 S,18.1 E in Figure 4b. After 40 days, Figure 4c. shows that this feature has propagated to 41.5 S,17.8 E, which yields a estimate for the phase speed of 0.8 km/day. Likely sources for these long waves are the maxima in the wind forcing near the Namibian coast at 25 S,8 E and 27.5 S,10 E, to the south of Cape Agulhas at 38 S,21 E, in mid-ocean at 37.5 S,9 W and along the 'roaring forties' particularly near 47 S,10 E (see section 5 for details). As a result of this number of wind maxima the model wave field shown here is somewhat more complex in its structure than that obtained by Cummins et al (1986) for the North East Pacific. Nevertheless, the same basic wave pattern of alternating crests and troughs in thermocline displacement is evident in Figures 4a.-c. Indeed, the wave pattern is coherently maintained for thousands of kilometres in the model domain. A tentative estimate for the wavelength of the waves
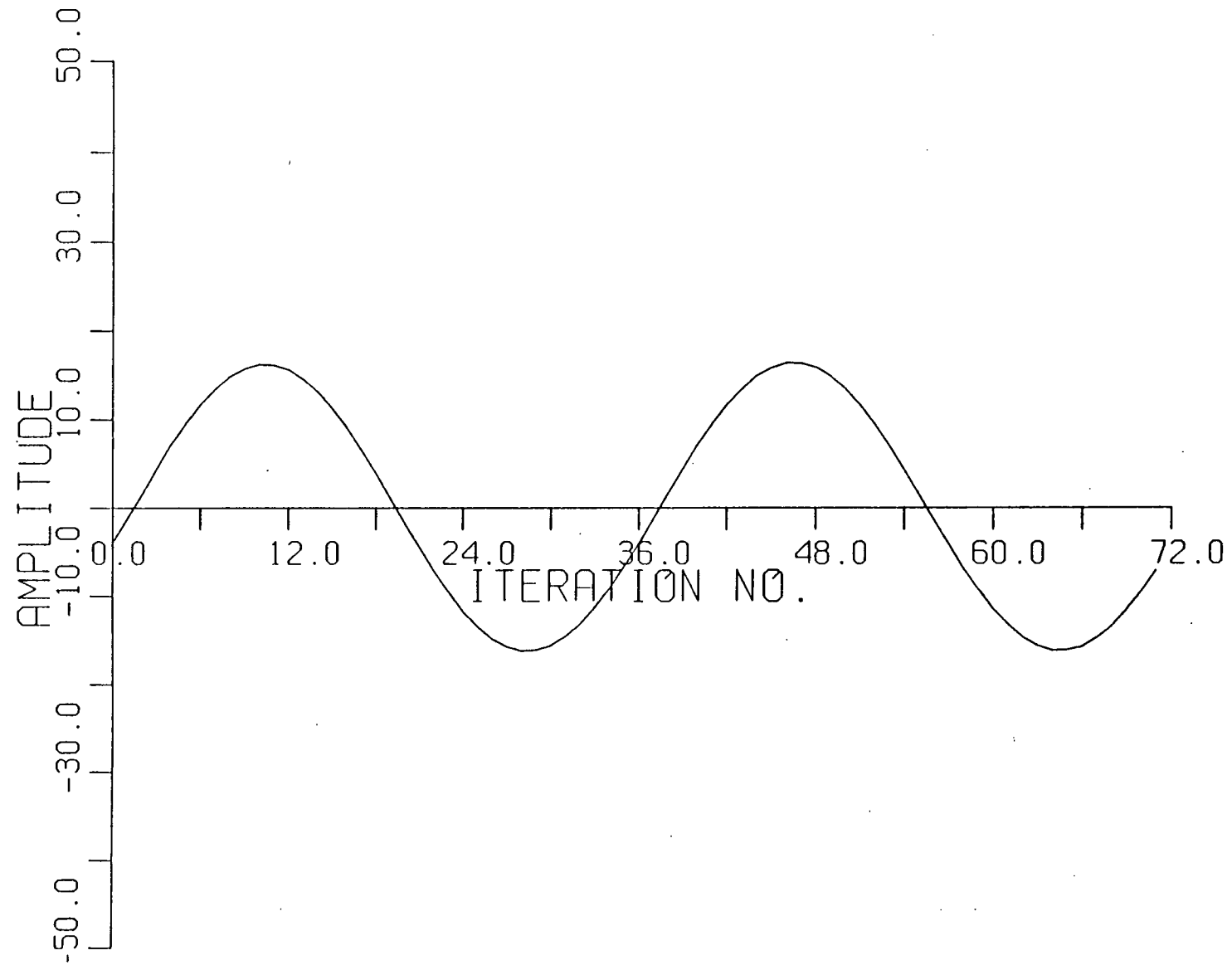
Figure 3. Example of steady state response of the model at the point 35 S,20 W.
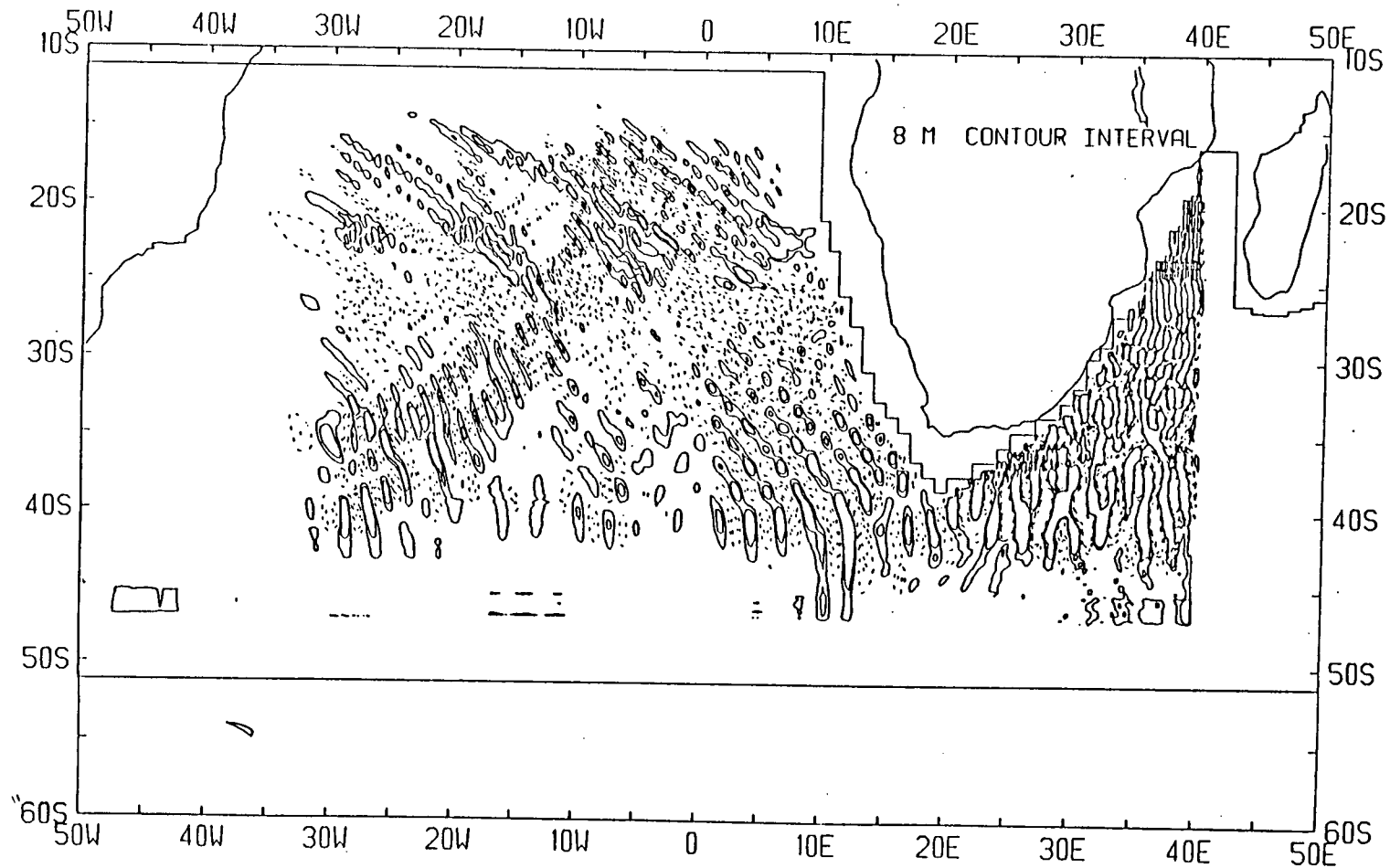
# Thermocline Height Anomaly



Figure 4a. Thermocline height distribution of the model in steady state response to the observed wind stress curl field.
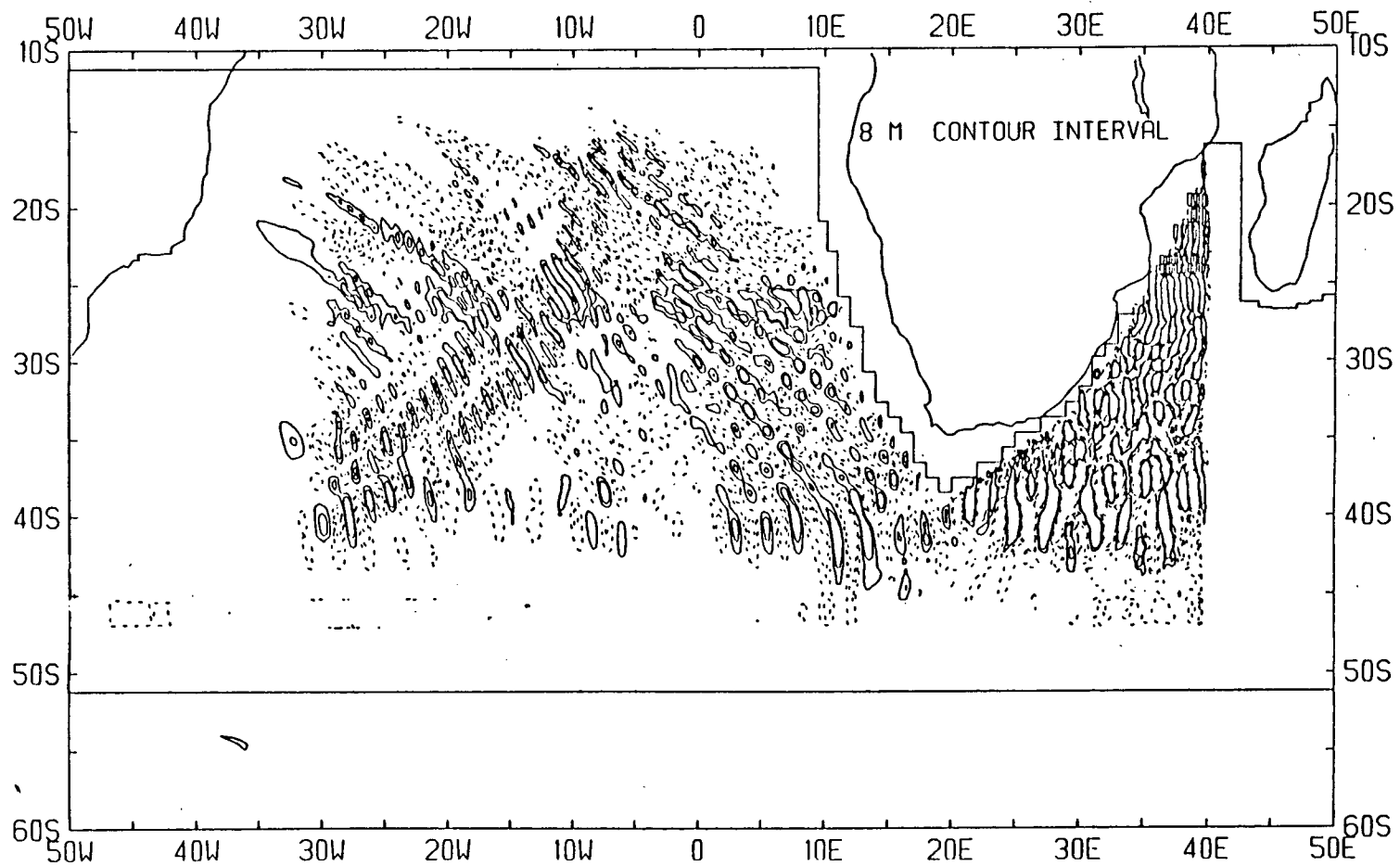
# Thermocline Height Anomaly



Figure 4b. The thermocline response 90 days (quarter phase) later.
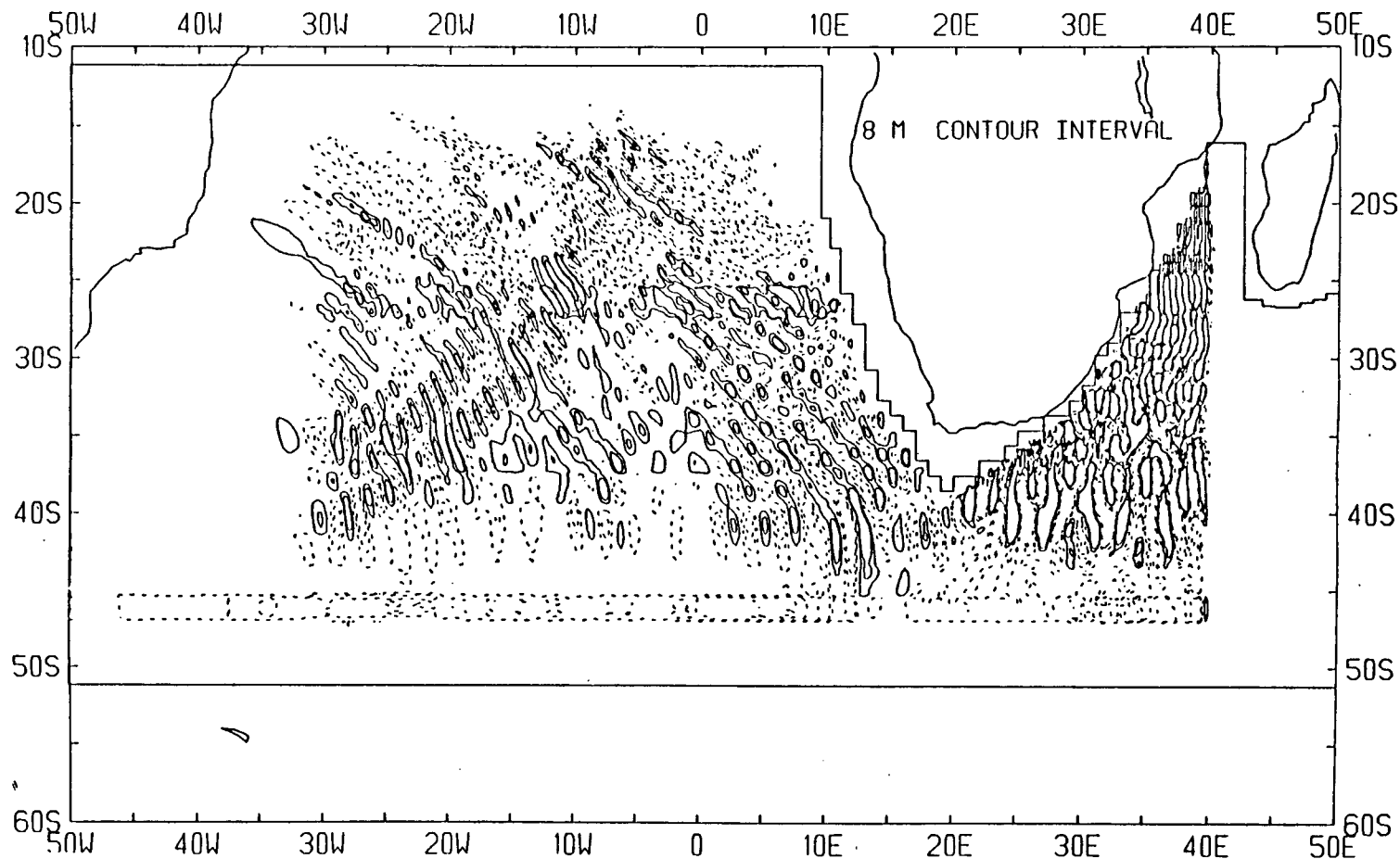
# Thermocline Height Anomaly



Figure 4c. The thermocline response 130 days (3/8 of a phase) later.

in mid-ocean of 400-500 km can be made. However a definite statement is only possible after detailed wave analysis (see section 5). Near the western coast of southern Africa the wave crests appear to be inclined roughly parallel to the land boundary i.e. in a NNW to SSE direction whereas further offshore the wave crests slope NW to SE or in a more zonal direction. As will be described later, this occurrence is a consequence of the refraction of the wave energy towards the equator as the waves propagate westwards across the ocean.

To the south and east of the land boundary the wave field appears to be even more complex. There are two areas of strong wind forcing which are likely to produce a significant wave response, namely, the maximum to the south of Cape Agulhas already mentioned and secondly that to the south west of Madagascar near 28 S,38 E. As Figures 4a.-c. show, the wave field in this region (the south west Indian Ocean) is far more densely packed than that in the South Atlantic Ocean and consists of short Rossby waves with eastward group velocity (the long Rossby waves in the South Atlantic have westward group velocity).

In addition, the nearby presence of the African landmass as a western boundary means that there is likely to be substantial reflection of these waves back into the south west Indian Ocean.The sharp cut-off in the thermocline response that is evident to the east of the 40 degree meridian marks the boundary of the wind forcing domain. To prevent any reflection of wave energy between this boundary and the African coastline there is a damping layer extending to 50 E - this is the eastern boundary of the model integration domain. It was felt that this approach was the best way of excluding any edge effects in the model while still being able to include the interesting model response immediately south east of the land boundary.

The action of the equatorial and western damping layers is also evident in the plots of the model response. Further north than 20 S, where the equatorial damping region begins, the waves emanating from the Namibian coast can be seen to be dissipated with increasing efficiency by the damping layer so that by the 15 S latitude there is little or no displacement of the thermocline. Similarly, to the west of the 26 longitude, the western damping region, which extends from here to the western boundary of the model domain

at 46 W, begins to attenuate the westward propagating waves effectively. Thus there is no wave energy evident beyond 34 W - the disturbances in the extreme south west of the domain are due to local Ekman pumping in response to the strong winds present there. The reason for imposing such a wide (20° ) damping layer here is in order to dissipate the waves completely before any energy can reach the South American continent near 40 W. In this way the question of Rossby wave reflection off this landmass is avoided. However, a drawback of having such a wide damping layer is that it may prevent any observation in the model response of refraction of wave energy propagating in a southwesterly direction towards the 47.2 S critical latitude back into the domain. For example, note how the pronounced wave motion near 44 S in the south west of the domain at 20 W to 30 W dies out very quickly. The situation in this area is complicated however by the presence of local Ekman pumping along much of the 45 S to 51 S band which is in response to the strong wind forcing ('the roaring forties') acting here (see Fig. 2a.). By Ekman pumping we mean the up and down motion of the thermocline forced by the winds but without the phase propagation characteristic of wave motion.

A final feature of the model Rossby wave field to be mentioned are the areas that are relatively quiet in terms of thermocline displacement. These are located around the points 35 S,7 W; 20 S,15 W and 43 S,30 E and correspond to the weak wind forcing present in these regions.

In summary, the model response consists of waves whose origins will be linked, in Section 5, with the observed maxima in the wind field. This result is to be expected as the governing equations of the model are linear. A good qualitative check can be seen in Figure 5 which shows the steady state response of the model to a small localised wind source. The winds were completely shut off over the whole domain except over the region 22 S to 28 S , 8 E to 0 E where they were set to a constant amplitude of $10.0 \times 10^{-9} dyne\,cm^{-3}$ (roughly corresponding to the wind peak offshore of the Namibian coast). After integrating out all the transients the resulting Rossby wave pattern is clearly to be seen. Several interesting points emerge from this study. Firstly, the waves increase in wavelength as they propagate
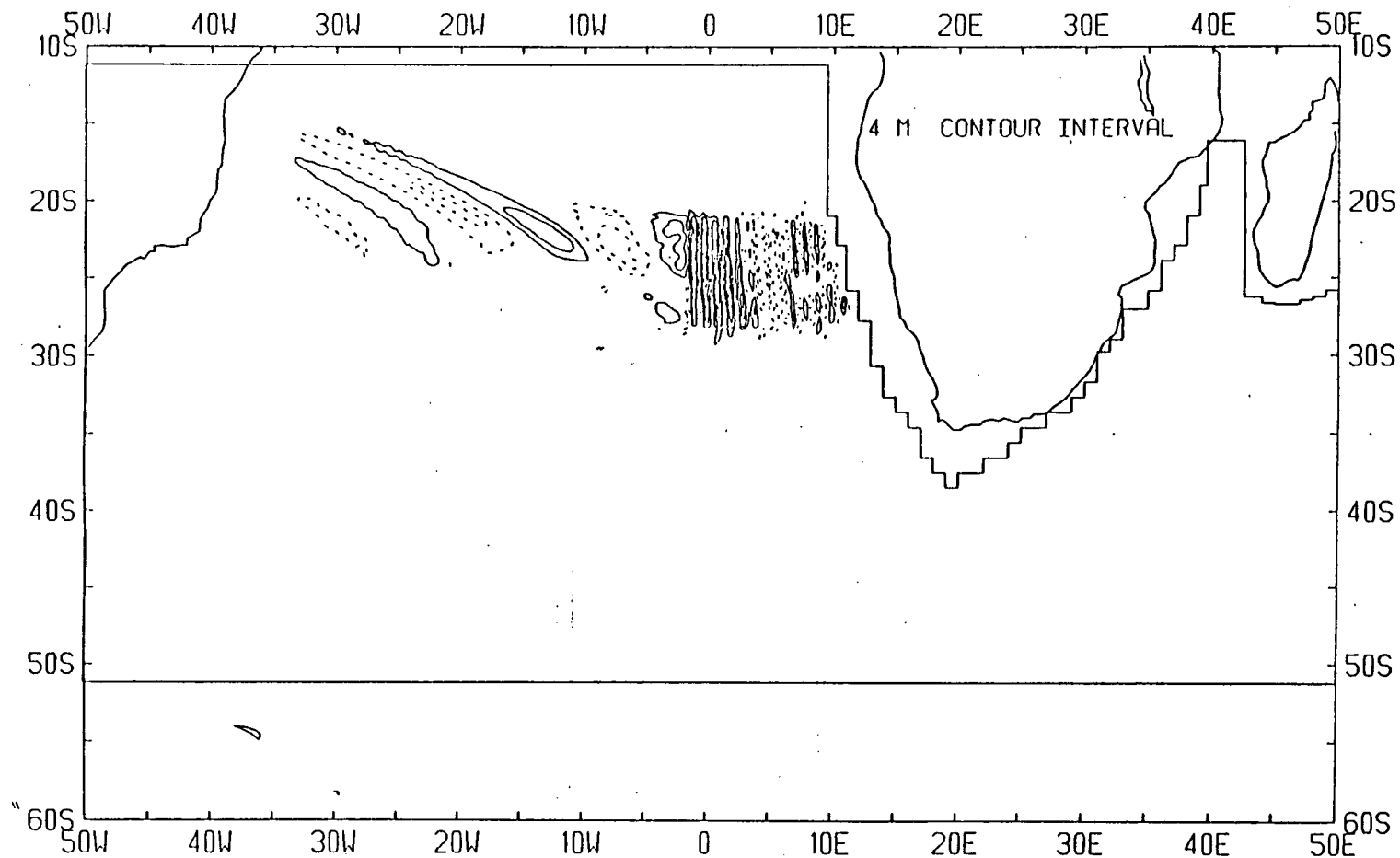
Figure 5. Steady state response of the model to an artificial wind forcing of $10 \times 10^{-9} dyne\ cm^{-3}$ over the region 22 S - 28 S,0 E - 8 E.

away from the generation area. Secondly, there is a bending of the wave crests towards the southwest. This is evidence of the refraction of the wave energy (as in the theory of Schopf et al, 1981) which initially has an approximately westward direction from the wind source towards the equator. Also, the wavelength is shorter near the equator which implies that the waves are slower here.

Although this type of check is useful for giving one an idea of what sort of results to expect from the model, to make any meaningful statements about how both the coast and mid ocean maxima in the wind field are forcing the model response one needs to determine the wavenumbers and direction of energy propagation of the waves in the relevant part of the field.

Before describing this detailed analysis it should be mentioned that one needs to be cautious when considering the shorter Rossby waves present in the model south west Indian Ocean. The reason is that the resolution of the model grid is 0.2 degrees (or 22 km approximately) which is approaching the wavelength of these waves and so the numerical solution is unlikely to be able to represent the dispersive nature of the waves with any reasonable accuracy. A useful paper concerned with this very point has been published recently by Wajsowicz (1986). She finds that the accuracy of using a finite difference grid for numerically modelling freely propagating Rossby waves depends on two non-dimensional resolution parameters in each spatial co-ordinate. Specifically, the wave resolution of a numerical model can be defined as the ratio of twice the grid spacing to the wavelength of the waves whereas the model grid resolution equals the grid spacing divided by twice the Rossby deformation radius. Both these parameters should be much less than unity for a realistic representation of the Rossby waves. Taking values appropriate to 15 S and 51 S (the boundary latitudes of the domain) yields grid resolutions of 21/145 and 14/48 respectively; both of which are much less than unity as required. Now the short waves evident in the model off the south eastern coast of Africa have a wavelength of about 50 km and so the short Rossby wave resolution in our model is roughly 44/50. Hence the accuracy of the finite difference representation of these waves is open to doubt. Also, the

presence of the strong poleward flowing Agulhas Current is likely to make non-linear effects (which have been ignored in our model) important. Hence, it is not meaningful to attempt a detailed analysis (e.g. wavenumber computations) for this part of the model ocean - only observations based on the latitude and longitude-time plots, to be described below, are possible. The main focus therefore, will be on the long waves propagating westwards across the South Atlantic Ocean. We take the longitude 25 E (near the Agulhas Bank) as the boundary between the two regions. Since the waves west of this longitude have wavelengths of hundreds of kilometres they should be effectively resolved by the model grid.

# 5. Analysis of the Rossby Wave Field

Direction of phase and energy propagation of the model waves :

In order to determine the likely sources of the waves together with their refractive and reflective properties, six plots of the thermocline anomaly distribution in both latitude-time and longitude-time space were made and the wavenumbers in the relevant parts of the field were computed. The latitude-time plots are considered first as they will indicate whether the generally westward propagating waves have any northward or southward component to their phase. The longitude-time plots are expected to confirm the westward phase required for a Rossby wave to propagate as well as indicate the zonal wavelength in different parts of the domain. With the general direction of phase determined by these plots it is then possible to deduce the general direction of energy propagation, i.e. the group velocity direction. This step is particularly important for the purpose of matching wave trains with sources as with such a complex wind stress curl field one must take care that the direction of the outwardly propagating energy from the wind stress curl maximum corresponds to the orientation of adjacent wave crests as closely as possible. It is most appropriate to use slowness curve theory to analyse the wave field as it not only enables the direction of wave energy and phase to be determined but also allows wave properties like refraction and reflection to be studied in a heuristic manner (see Mysak (1983) for an example of its application to the propagation of Rossby waves in the North Pacific). To apply the slowness curve theory one must assume that once the wave disturbances have left the coastal ocean and do not encounter any offshore vorticity sources, they can be treated as freely propagating nearly plane waves. The slowness curve is defined as a curve of constant frequency $\omega$ in wavenumber $\underline{k}$ space and so its derivation follows from the dispersion relation $\omega = \omega(\underline{k})$ for the waves (see the Appendix for details). The result is a circle of radius $r = \sqrt{((\frac{\beta}{2\omega})^2 - R^{-2})}$ and centre $(k,l) = (-\frac{\beta}{2\omega}, 0)$ where $\underline{k} = k\underline{i} + l\underline{j}$ and $R^2 = g'H_o f^{-2}$ is the square of the Rossby deformation radius. For future reference note that these formulae are used to determine the appropriate radii and centres of the slowness circles to be described below.

We now consider the relevant slowness curves for several different areas in the model domain; namely near the Namibian coast at 23 S,2 E, in mid South Atlantic Ocean around 33 S,20 W and at 40 S,20 W, to the south east of Cape Agulhas near 38 S,30 E and finally east of the South African coast at about 32 S,35 E. In each case the slowness curve consists of a circle of the appropriate radius centred on a beta plane at the given latitude.

<u>Case 1 :Near the Namibian coast :</u>

Figure 6a is a latitude-time plot taken along the 2 E meridian. Phase is seen to propagate from the west coast of Southern Africa with a southward component (because of the negative slope of the plot. For example the dashed line shows that a wave front at 25 S on day 0 has propagated to 26 S by day 300). Because the waves are transverse the phase velocities and hence the wavenumbers are normal to the coast. The corresponding slowness diagram (the top circle in Figure 7a.) shows the wavenumber vector associated with the group velocity drawn towards the centre of the circle from where the phase wavenumber vector meets the circumference. Hence the group velocity and therefore the the wave energy are directed slightly to the north of west. Consequently, the source for these waves must be the wind maxima located off the Namibian coast near 25 S,8 E. Let us now determine how this equatorward transport of wave energy affects the slowness characteristics. From equations (A.6) and (A.9) the dispersion relation and group velocity are

$$\omega = -\frac{\beta k}{(k^2 + l^2 + R^{-2})}$$

$$\underline{c}_g = \frac{\beta}{(k^2 + l^2 + R^{-2})^2}(k^2 - (l^2 + R^{-2}), 2kl)$$

where $\beta = 2\Omega \cos\theta_o/a$ and $f = f_0 + \beta y$, $\Omega$ is the earth's rotation rate, $\theta_o$ is the mean latitude and y is the distance north from this latitude.

On a beta plane the Coriolis parameter and l are slowly varying functions of y along group velocity vectors whereas $\omega$ and k are constants (Schopf et al, 1981). Therefore as $f^2$ decreases towards the the equator $l^2$ must increase so as to conserve $\omega$ and k. Similarly, $l^2$ must decrease as one moves towards the pole. Also, the ratio of the group velocity
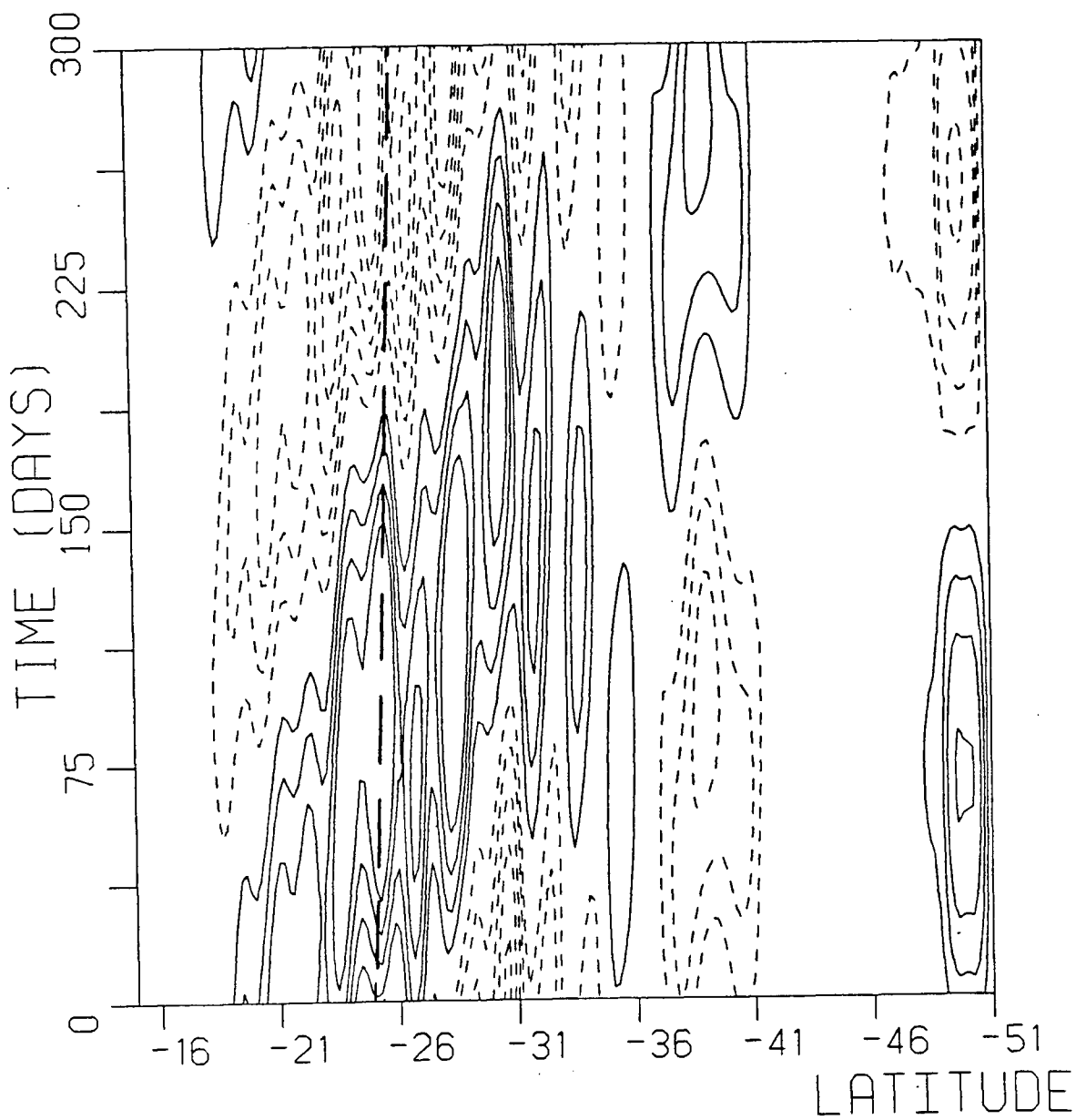
Figure 6a. Latitude-time plot of the thermocline height field for 2 E. The negative slope of the straight dashed line indicates a southward component of phase propagation. Contour interval is 4m.
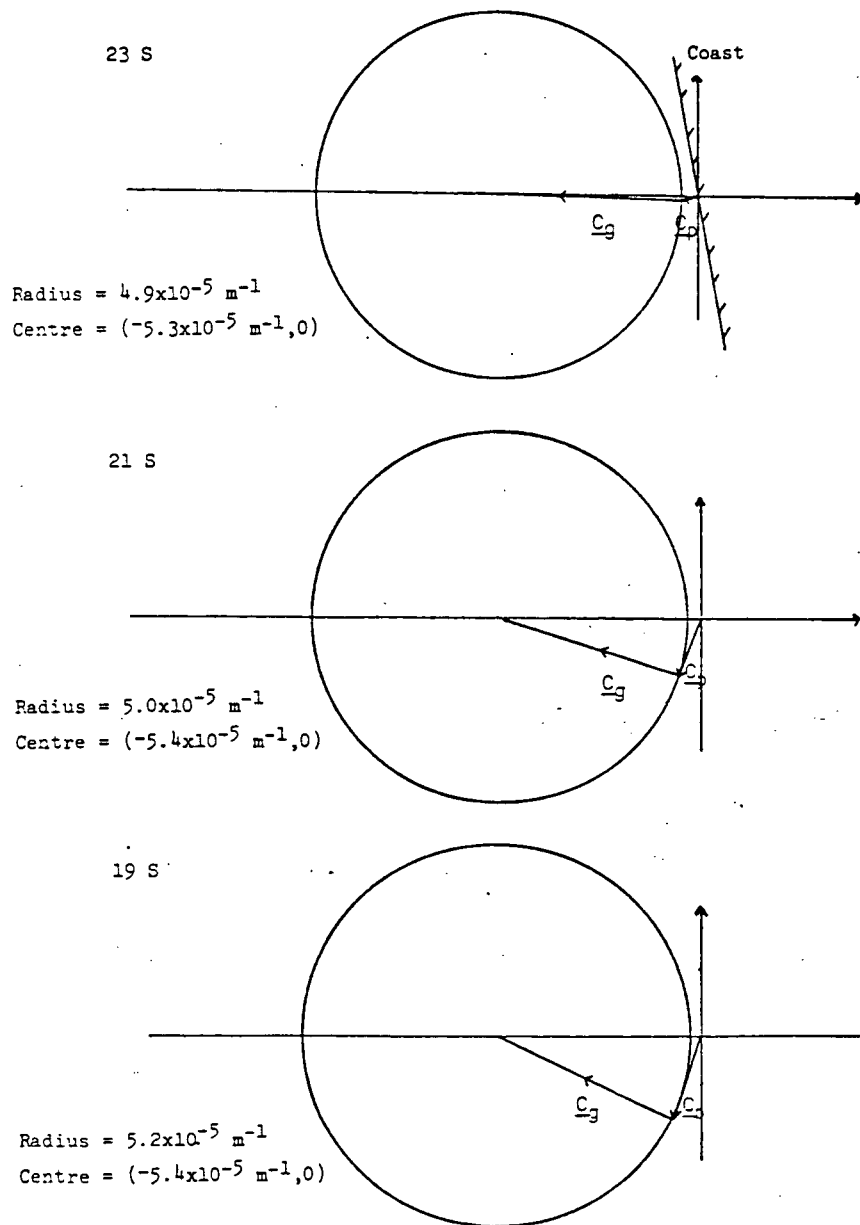
23 S

Coast

Radius = $4.9 \times 10^{-5}$ $m^{-1}$
Centre = $(-5.3 \times 10^{-5}$ $m^{-1}, 0)$

$\underline{C}_g$
$\underline{C}_p$

21 S

Radius = $5.0 \times 10^{-5}$ $m^{-1}$
Centre = $(-5.4 \times 10^{-5}$ $m^{-1}, 0)$

$\underline{C}_g$
$\underline{C}_p$

19 S

Radius = $5.2 \times 10^{-5}$ $m^{-1}$
Centre = $(-5.4 \times 10^{-5}$ $m^{-1}, 0)$

$\underline{C}_g$
$\underline{C}_p$

Figure 7a. Slowness curve showing refraction of wave energy starting near 23 S,2 E. Time history of the slowness circles is from top to bottom.

components

$$\frac{|c_{gl}|}{|c_{gk}|} = \frac{2kl}{k^2 - l^2 - R^{-2}}$$

increases towards the equator. Thus a group velocity in the WNW direction in the Southern Hemisphere will tend to be refracted further north or towards the equator.

In addition, the radius r of the slowness circle increases as $f^2$ decreases towards the equator so that as the group velocity vector turns clockwise in this direction, the phase velocity turns more and more to the southwest (see the lower two circles in Fig. 7a.) and its magnitude, which is inversely proportional to the wavenumber, decreases. In other words as the waves travel towards the equator they slow down. This behaviour is in complete contast to the situation in the North Pacific where a coastline of similar orientation to the Namibian results in waves initially propagating phase to the southwest and energy slightly to the north of west, i.e. polewards. Thus, for the North Pacific case the slowness circle decreases in radius to a point where both the group and phase velocities are purely zonal. Refraction of energy equatorwards continues and so causes the curve to begin expanding again. The result is that these long and nearly zonal waves increase in speed nearer the equator (see Cummins et al (1986) for details) whereas for the shorter waves in this part of the South Atlantic the reverse holds true.

Further south along the 2 E meridian, Figure 6a. shows the phase also to have a poleward component as far as 40 S. Applying the same slowness curve argument indicates that the wave energy is again transported in northwesterly direction. A possible source for this energy is the 'roaring forties' near 46 S,10 E. Indeed as the thermocline anomaly plots (Figs. 4a. and b.) and the latitude-time plot for 15 E (Fig 6e. on page 32) show, these poleward propagating waves extend from at least 15 E in a coherent train to 0 E before merging with other wave sets. Between 41 S and the critical latitude there is no wave activity as is confirmed by the thermocline anomaly distribution in Figure 4a. The closed contours around 50 S are evidence of Ekman pumping.
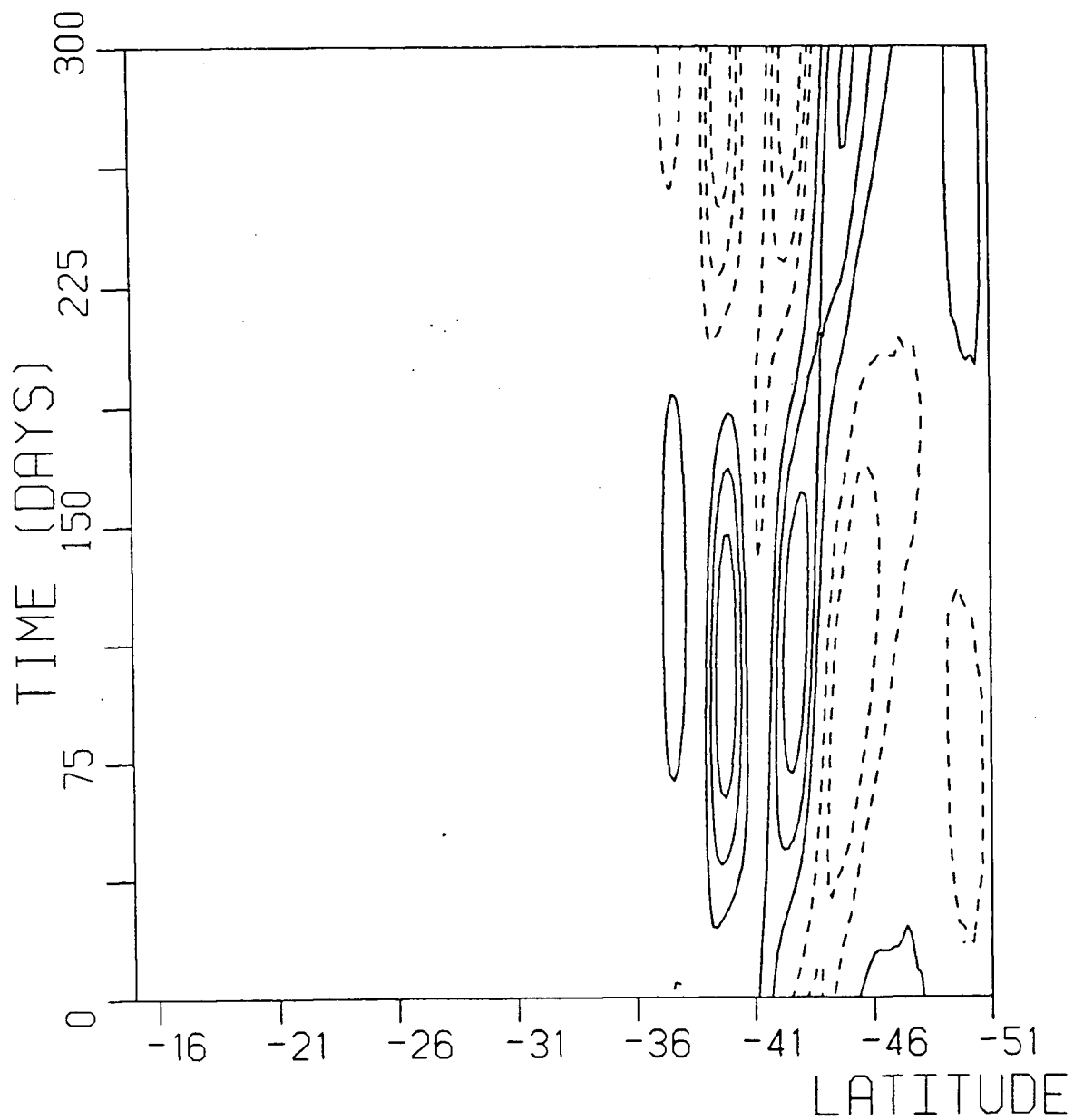
Figure 6e. Latitude-time plot of the thermocline height field for 15 E. Contour interval is 4m.

## Case 2 : South Atlantic Ocean between 12 W and 30 W :

Since the waves at this location are well away from any coastlines it is not as simple as for the case above to determine the initial direction of the phase. Although the waves must have a basically westward direction it could be biased in either a northwards or southwards direction. Figure 6b. indicates that the phase at 20 W must have a small northward component between 30 S and 34 S. From the slowness curve (Fig. 7b.) the group velocity is initially slightly south of west which suggests that the wave energy has arisen from the Namibian coastal source. Since the initial wave energy transport is polewards the slowness circle local to the disturbance shrinks in size. However, refraction of this energy equatorwards and conservation of the zonal wavenumber mean that the group velocity and phase become increasingly zonal in direction until a point is reached where the circle is at its minimum radius and both vectors are entirely westward in direction. This latitude marks the furthest south that the wave disturbance reaches. Thereafter, continued refraction equatorwards causes the group velocity to rotate clockwise to a northwest direction, the phase becomes southwest and the circle expands again. It is difficult to see whether this process is actually occurring in the thermocline plots because the friction zone which extends to 26 W would actively damp out these waves. Further south between 36 S and 40 S Figure 6b. shows that there are poleward propagating waves. Since these waves must have a northwest direction of group velocity it follows that they are likely to be generated by the strong zonal winds (the 'roaring forties') which extend from the bottom of the domain as far as 46 S.

Further west at 30 W, Figure 6c. shows southward propagating waves with associated equatorward direction of group velocity between 15 S and 31 S. Hence, a likely source for these waves is the maxima in the wind field in mid-ocean near 38 S,21 W.

Along 12 W, there is again more than one set of waves. Figure 6d. shows a southward component of phase between 15 S and 36 S whereas between 38 S and 42 S the waves are
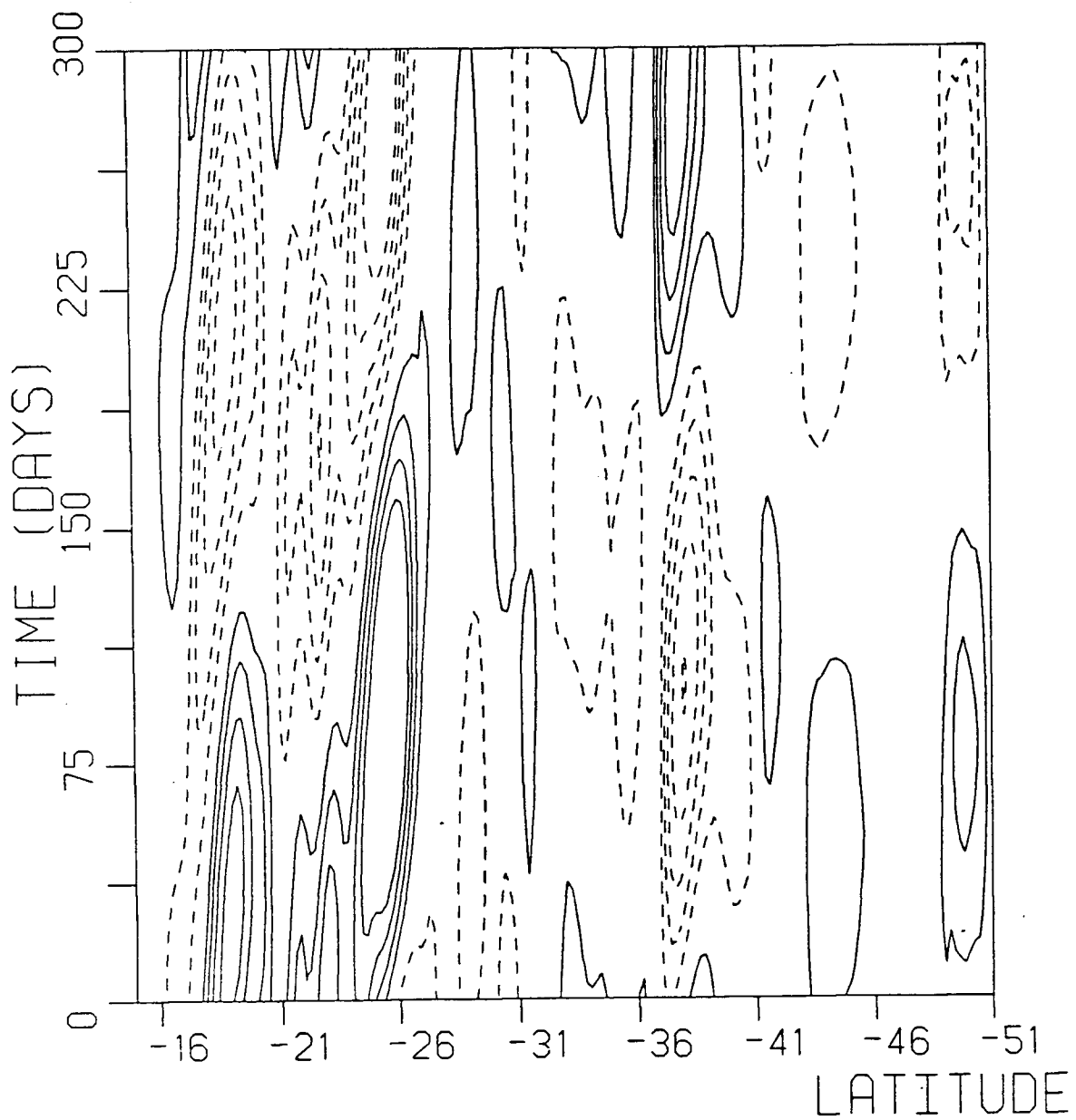
Figure 6b. Latitude-time plot of the thermocline height field for 20 W. Contour interval is 4m.
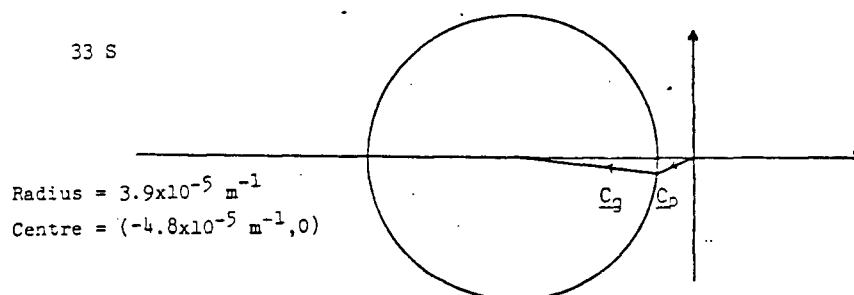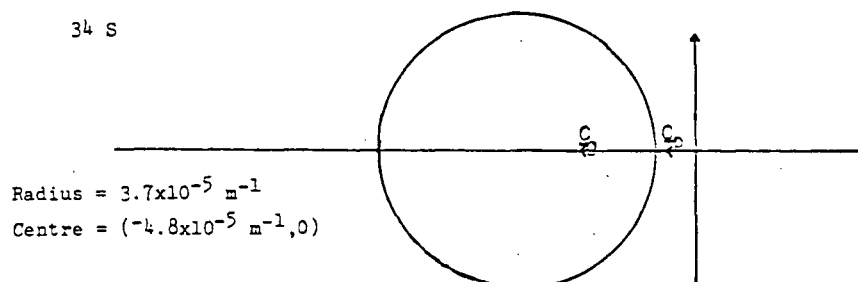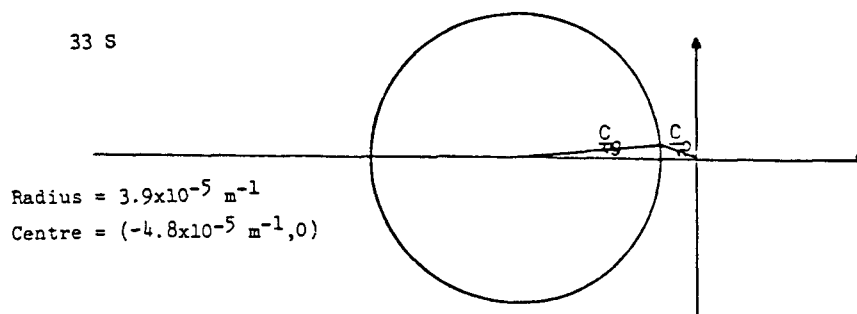
33 S

Radius = $3.9 \times 10^{-5}$ m$^{-1}$
Centre = $(-4.8 \times 10^{-5}$ m$^{-1}, 0)$

34 S

Radius = $3.7 \times 10^{-5}$ m$^{-1}$
Centre = $(-4.8 \times 10^{-5}$ m$^{-1}, 0)$

33 S

Radius = $3.9 \times 10^{-5}$ m$^{-1}$
Centre = $(-4.8 \times 10^{-5}$ m$^{-1}, 0)$

Figure 7b. Slowness curve showing refraction of wave energy starting near 33 S,20 W. Time history of the slowness circles is from top to bottom.
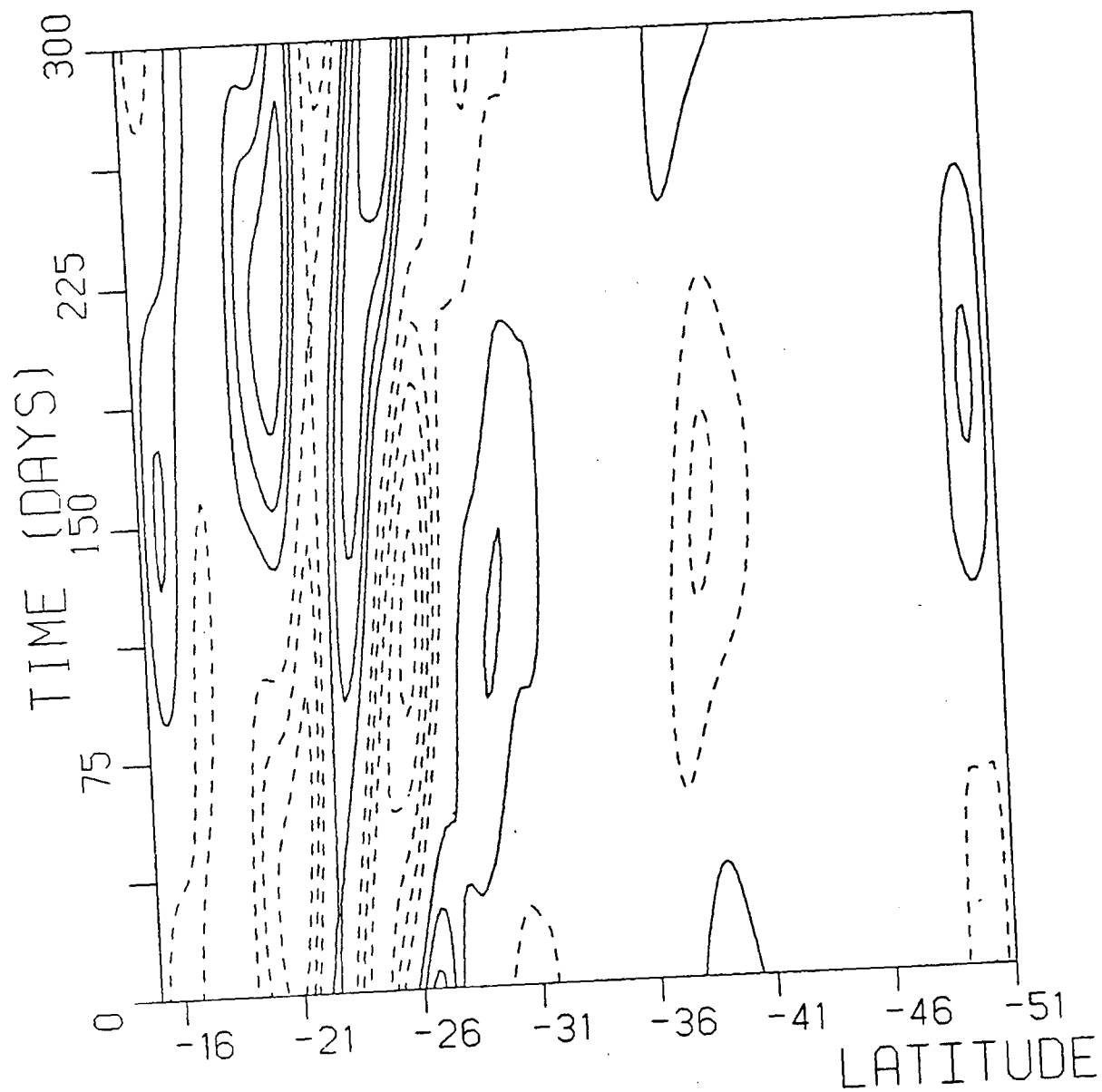
Figure 6c. Latitude-time plot of the thermocline height field for 30 W. Contour interval is 4m.
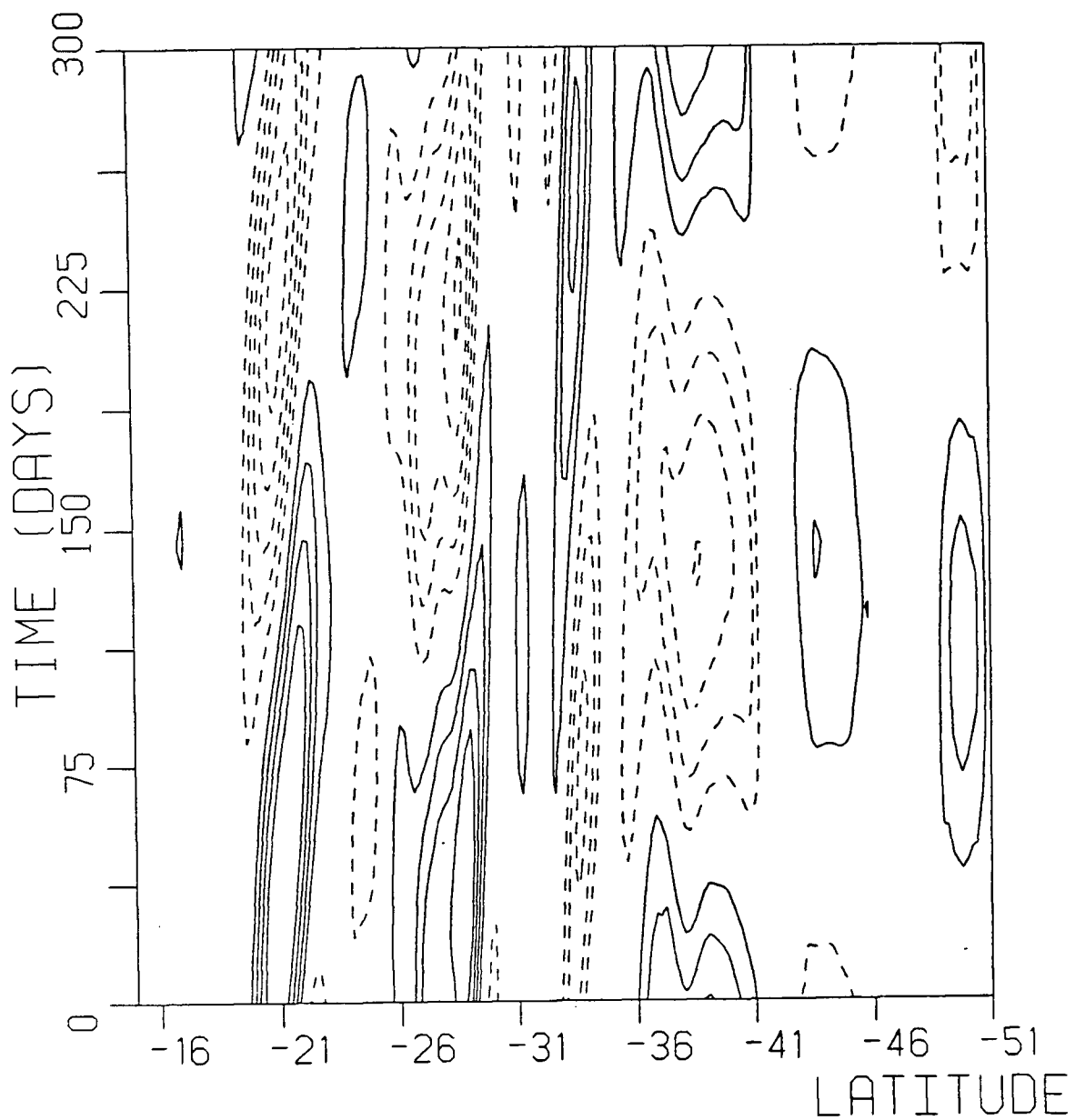
Figure 6d. Latitude-time plot of the thermocline height field for **12 W**. Contour interval is **4m**.

virtually zonal in direction. Applying the same arguments as above indicates that the first set of waves likely arises from the mid ocean source near 38 S,8 W (with northwestward group velocity) whereas the higher latitude waves probably arise from the source near the Agulhas Bank.

<u>Case 3 : South East of Cape Agulhas :</u>

Before considering the application of the slowness curve theory to the short waves evident off the south eastern coast of Southern Africa it should be emphasised that both this theory and the model equations have assumed a zero mean flow. Obviously, the presence of the intense poleward flowing Agulhas Current in the South West Indian Ocean would in practice make the observation of any Rossby waves virtually impossible. As far as the slowness curves are concerned however, the qualitative results described above for the South Atlantic would only hold for relatively long waves. In the case of a mean flow the dispersion relation in the short wave regime is considerably changed, leading to a slowness curve which is approximately elliptical in shape (Kang and Magaard, 1980). Nevertheless, we consider the zero mean flow case as it is useful for the purpose of studying possible reflection of wave energy off the western boundary (the east coast of Southern Africa).

Figure 6f. suggests that the waves between 37 S (roughly where the land ends) and 39 S along 30 E have a poleward component and are short as indicated by the narrow spacing between the contours in the figure. The short wavelength is also confirmed by the narrow spaced contours of the longitude-time distribution at this location (Fig. 8a. - page 40). The slowness circle (Fig. 7c. - page 41) shows that the group velocity is north eastward so it is probable that these waves arise from the strong winds near the Agulhas Bank. It is also interesting to note how at higher latitudes in Fig. 6f. the waves become increasingly zonal until by 40 S the phase has a slight northward component corresponding to a group velocity with a slight southward component (Fig. 7d. - page 42). This behaviour is consistent with the Agulhas Bank wave source. Further east along 35 E, Figure 6g. (page 43) shows that there are equatorward propagating waves between 29 S and 33 S. The corresponding slowness circle (Fig. 7e.) indicates that wave energy from
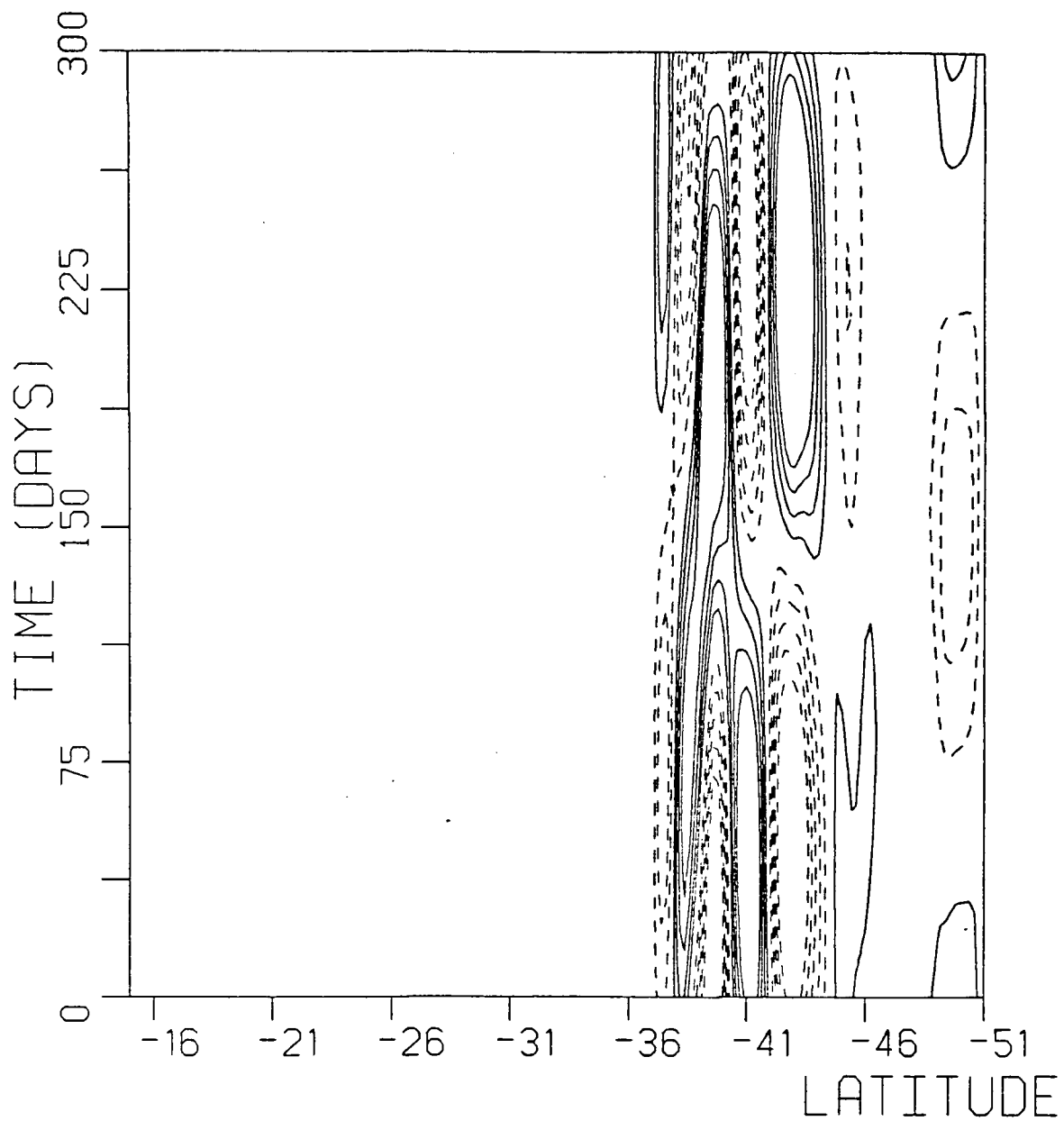
Figure 6f. Latitude-time plot of the thermocline height field for 30 E. Contour interval is 4m.
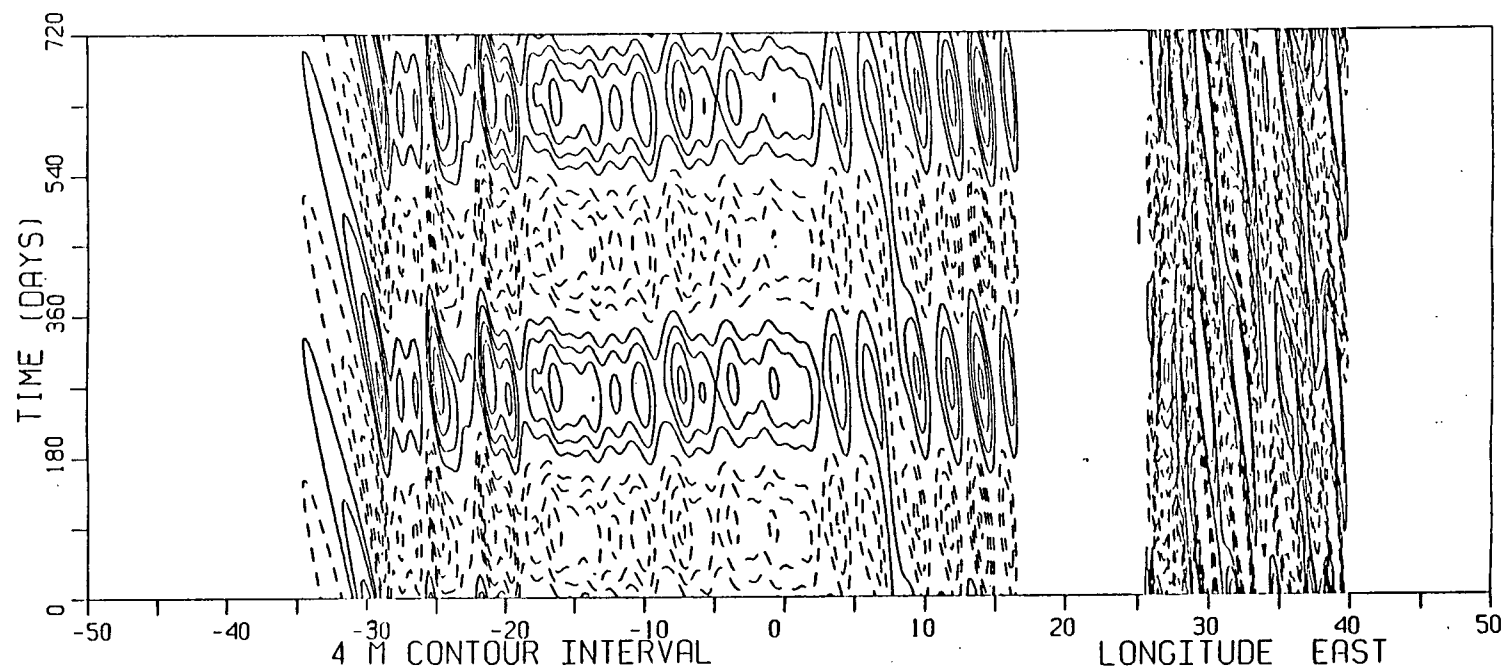
**Figure 8a. Longitude-time plot of the thermocline height field along 40 S.**

38 S

Radius = $3.1 \times 10^{-5}$ m$^{-1}$
Centre = $(-4.5 \times 10^{-5}$ m$^{-1}, 0)$

$\underline{C}_g$  $\underline{C}_p$

33 S

Coast

Radius = $3.9 \times 10^{-5}$ m$^{-1}$   R
Centre = $(-4.8 \times 10^{-5}$ m$^{-1}, 0)$

$\underline{C}_{gr}$

$\underline{C}_{gi}$  $\underline{C}_{pi}$

I

31 S

Radius = $4.1 \times 10^{-5}$ m$^{-1}$
Centre = $(-4.9 \times 10^{-5}$ m$^{-1}, 0)$
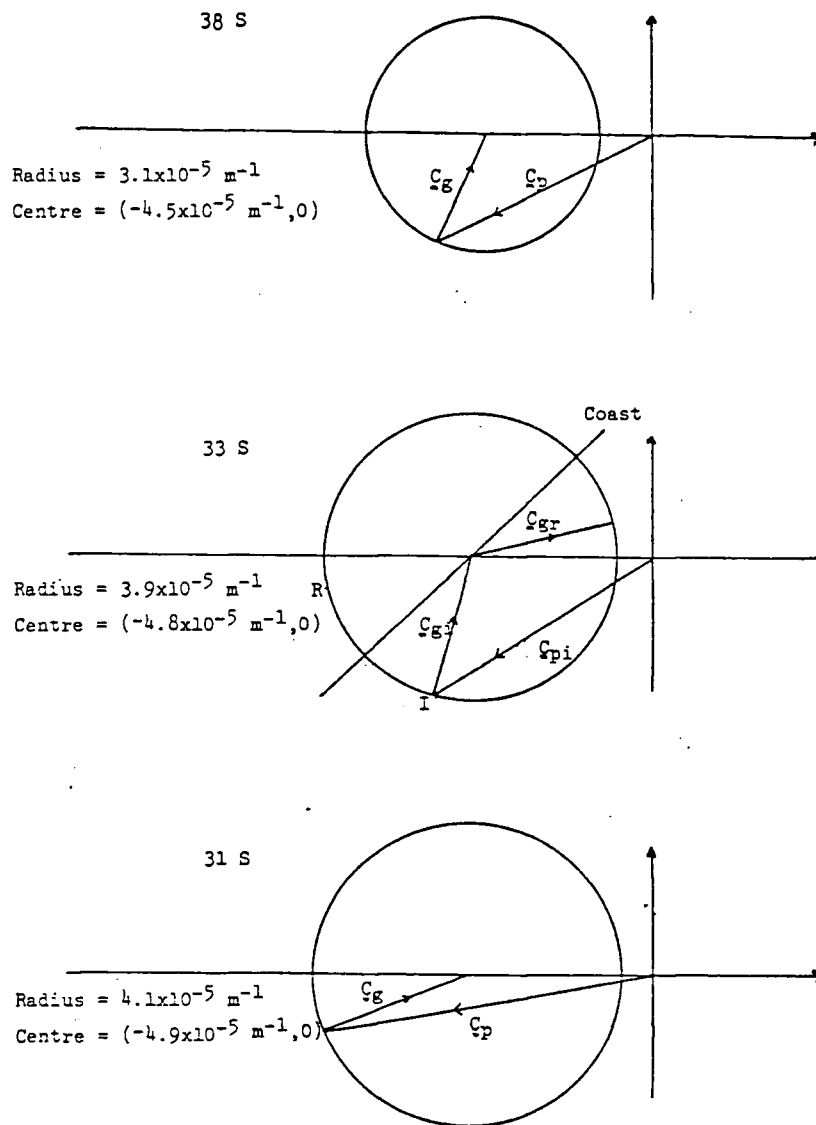
$\underline{C}_g$  $\underline{C}_p$

Figure 7c. Slowness curve showing reflection and subsequent refraction of wave energy near 33 S,30 E. Time history of the slowness circles is from top to bottom.

41

40 S

Radius = $2.8 \times 10^{-5}$ m$^{-1}$

Centre = $(-4.4 \times 10^{-5}$ m$^{-1},0)$

$C_p$

$C_g$

41 S

Radius = $2.6 \times 10^{-5}$ m$^{-1}$

Centre = $(-4.3 \times 10^{-5}$ m$^{-1},0)$

$C_p$

$C_g$

39 S

Radius = $3.0 \times 10^{-5}$ m$^{-1}$

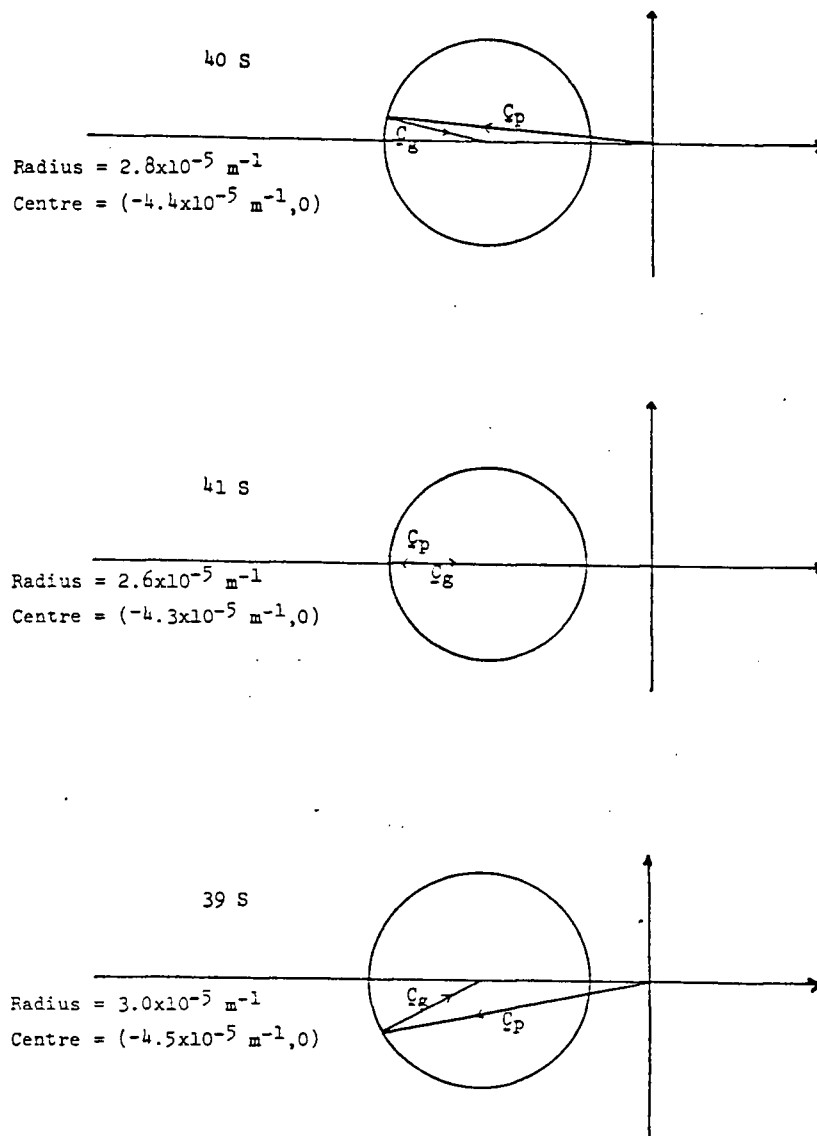Centre = $(-4.5 \times 10^{-5}$ m$^{-1},0)$

$C_g$

$C_p$

Figure 7d. Slowness curve showing refraction of wave energy near 41 S, 30 E. Time history of the slowness circles is from top to bottom.

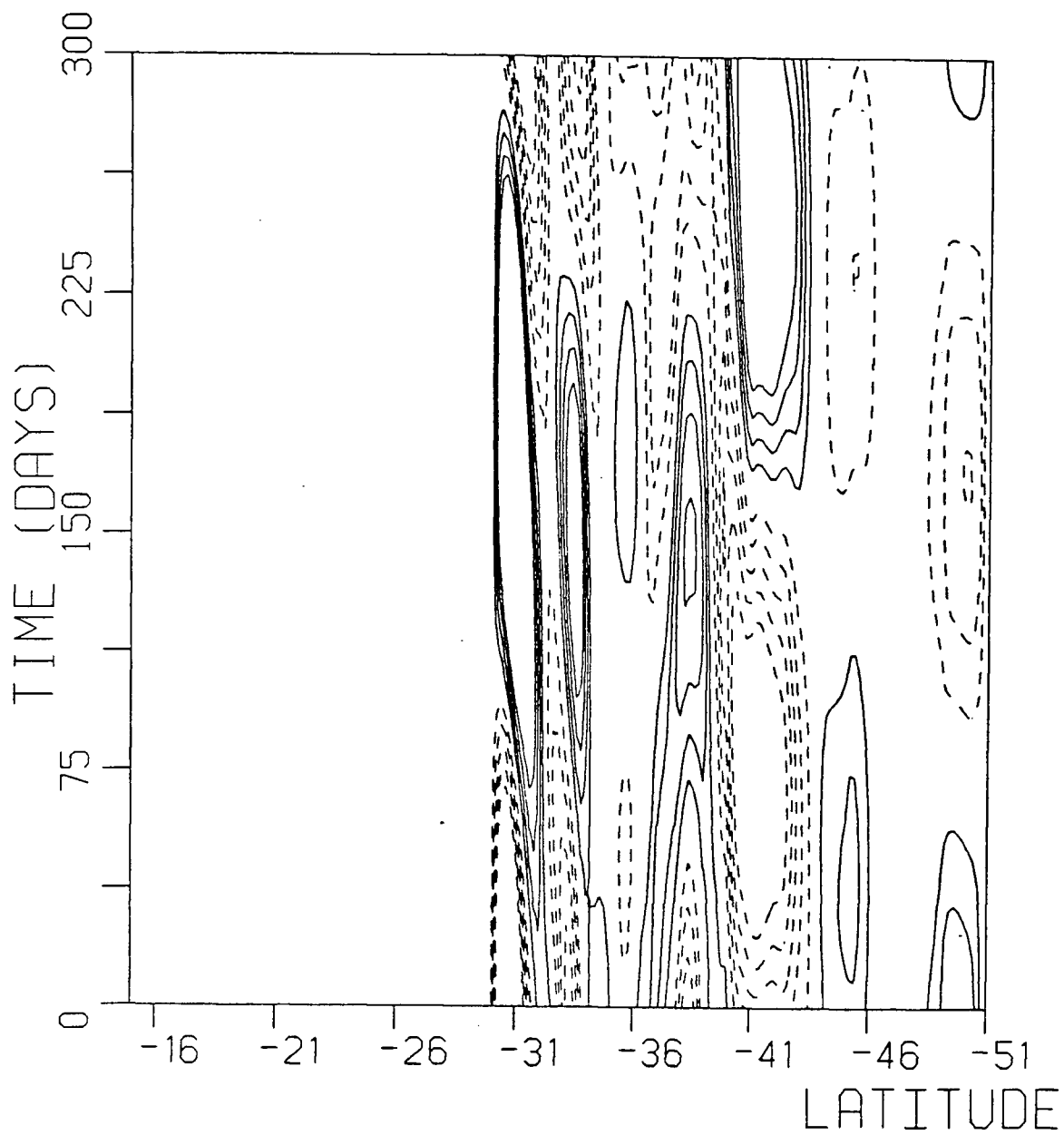Figure 6g. Latitude-time plot of the thermocline height field for 35 E. Contour interval is 4m.

30 S

Radius = $4.2 \times 10^{-5}$ m$^{-1}$
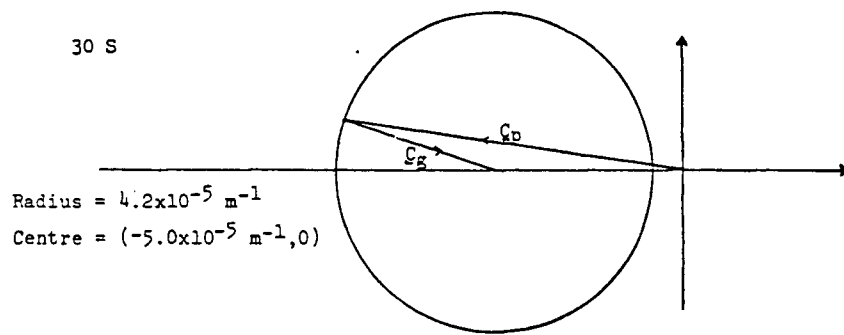Centre = $(-5.0 \times 10^{-5}$ m$^{-1}$,0)

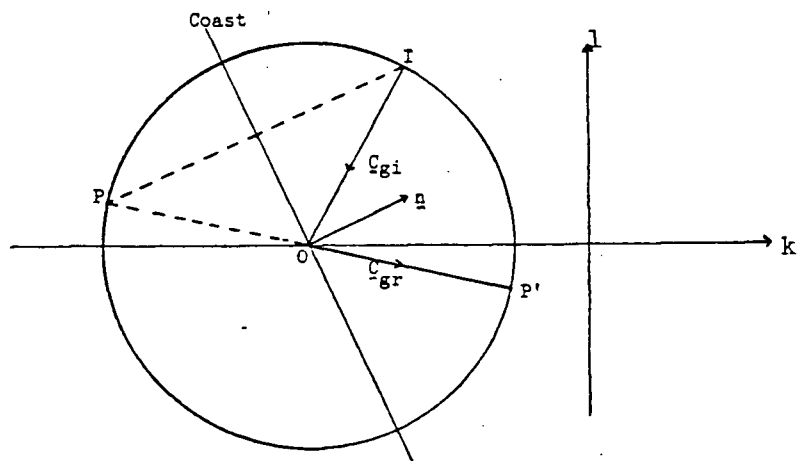Figure 7e. Slowness curve showing direction of wave energy propagation near 30 S,35 E.

Figure 7f. Slowness curve showing reflection of wave energy off an idealised wall.

these short waves must come from near the Natal/Mozambique coast as the group velocity is southeasterly. A glance at the wind field (Figure 2a.) shows that there are indeed strong winds ($(15-20) \times 10^{-9} dyne\ cm^{-3}$) along this coast between 24 S and 31 S.

Because of the nearby location of Africa as a western boundary to these waves the possibility of reflection arises. To decide whether this is a realistic possibility we consider the generally WSW to ENE orientation of this coast together with the direction of the group velocity of each wave set. Clearly, the waves between 39 S and 46 S with their eastward or southeastward energy propagation cannot be reflected. Instead, Fig. 7d. shows that the local slowness circle shrinks as they propagate polewards. Continual refraction of the energy towards the equator causes the circle to pass through a minimum radius (at the southernmost point that the waves reach) before expanding again with an associated energy transport northeastwards into the Indian Ocean. Similarly, the short waves originating near the Natal coast are unlikely to be reflected and will, like the high latitude waves, go through the same sequence of shrinking and expanding slowness curves as they are refracted equatorwards.

At 37 S however, energy is being transported with a large northward component so it is feasible that reflection could occur as illustrated in Fig. 7f. This diagram has been derived using the following properties of Rossby waves (see LeBlond and Mysak, 1978). Firstly, the group velocity satisfies Snell's law of reflection so that the angle of incidence equals the angle of reflection. Secondly, the reflected wave amplitude has the same magnitude as the incident amplitude but a phase change of $180^{o}$ occurs upon reflection for the phase velocity. Also, one need not worry about the wavelength of the waves as the reflection characteristics for Rossby waves are identical for both the short and the long wave. The reason is that, as will be shown below, the reflection coefficient and change in phase are independent of the wavelength.

Let $h_i = A(x,y,t)exp(i(k_1 x + k_2 y - \omega t)$ be the incident wave.

and $h_r = RA(x,y,t)exp(i(l_1 x + l_2 y - \sigma t)$ be the reflected wave.

where R is a reflection coefficient. Note that the general dispersion relation (A.6) is

satisfied by both waves. The boundary condition at the land, $h = 0$, will determine how the reflected wave will propagate. For simplicity, we approximate the slope of the coastline by the straight line $y = ax$, where a is a constant. Substituting the two wave forms into the boundary condition yields

$$exp(i(k_1 + ak_2)x - \omega t) + Rexp(i(l_1 + al_2)x - \sigma t) = 0$$

This result holds for all x and t if $\sigma = \omega$, $l_1 + al_2 = k_1 + ak_2$ and $R = -1$. Hence the reflected wave amplitude equals that of the incident wave, but there is a 180 degree phase change upon reflection. Since the incident and reflected frequencies are the same both waves must satisfy the same slowness circle. The second result implies that the reflected phase velocity is a mirror image about the coastline of the incident wave which meets the circle at I in Figure 7f. Hence it follows that the group velocity of the reflected wave $c_{gr}$ is in the direction $POP'$ away from the wall such that angle $nOI$ (incidence) equals angle $nOP'$ (reflected) i.e. Snell's law holds.

One can also show that the energy flux normal to the boundary has its magnitude conserved but its direction reversed. Another interesting property occurs for nearly non-divergent Rossby waves i.e. those waves satisfying $k_1^2 + k_2^2 >> R^{-2}$. For this case the magnitude of both the incident and the reflected group velocities are inversely proportional to the square of their respective horizontal wavenumbers. Thus,

$$|c_{gi}|\alpha k^{-2}, \ k^2 = k_1^2 + k_2^2$$

*and*

$$|c_{gr}|\alpha l^{-2}, \ l^2 = l_1^2 + l_2^2$$

However as LeBlond and Mysak (1978) show, the energy density satisfies

$$< E_i(k) > \alpha k^2 \quad and \quad < E_r(l) > \alpha l^2$$

so that the energy flux $|c_g| < E >$ is independent of wavenumber magnitude and hence the wavelength. These results indicate that one might expect to find small scale wave energy

concentrated near the western boundary of an ocean. Figure 7f. shows how this concentration might occur. A relatively long incident wave with westward energy propagation is reflected back as a shorter wave with eastward propagating energy. This effect will be even more pronounced for a boundary aligned North-South rather than the ESE-WNW one shown. Since $< E > \alpha k^2$, the fact that $k^2 < l^2$ indicates that the reflected wave has more energy and so the western boundary could act as a source of small scale, highly energetic wave motions (in other words there is a westward intensification of wave energy). Unfortunately, it is not likely that the model results will display this feature as a long wave with westward energy propagation is nowhere allowed to reach a western boundary in the model. Near the South American boundary the western sponge layer prevents reflection whereas off the east coast of Africa the model domain and wind field is too narrow in extent to permit long waves to be generated. Nevertheless, let us consider how the relatively short to medium length waves (see the longitude-time plot Figure 8b. for an indication of the wavelength) present there may reflect. The second circle in Fig. 7c. illustrates the application of the above principles to the coastal ocean near 33 S,30 E. A medium length wave meets the circle at point I resulting in a group velocity with a large northward component. After undergoing reflection the wave is somewhat shorter in wavelength (it meets the circle at point R) and has a group velocity that is eastnortheasterly in direction. Hence it is still possible that the intensification of energy described above may occur. In addition the reflected group velocity with equatorward direction will be refracted still nearer the equator so that the local slowness circle expands (see the third circle in Fig. 7c.). Hence, like the wave sets both to the north and the south described earlier, there is a general energy flux northeastward into the Indian Ocean with a possible concentration near Madagascar. Although the model domain does in fact extend to 50 E which is east of this island, the sponge layer between 40 E and 50 E prevents observation of this process in the model results. Of course, as has been discussed above, the presence of the Agulhas Current may in reality make such a possibility academic. SEASAT Altimeter data for the area shows substantial mesoscale (i.e. Rossby wave scale) variability in the South West
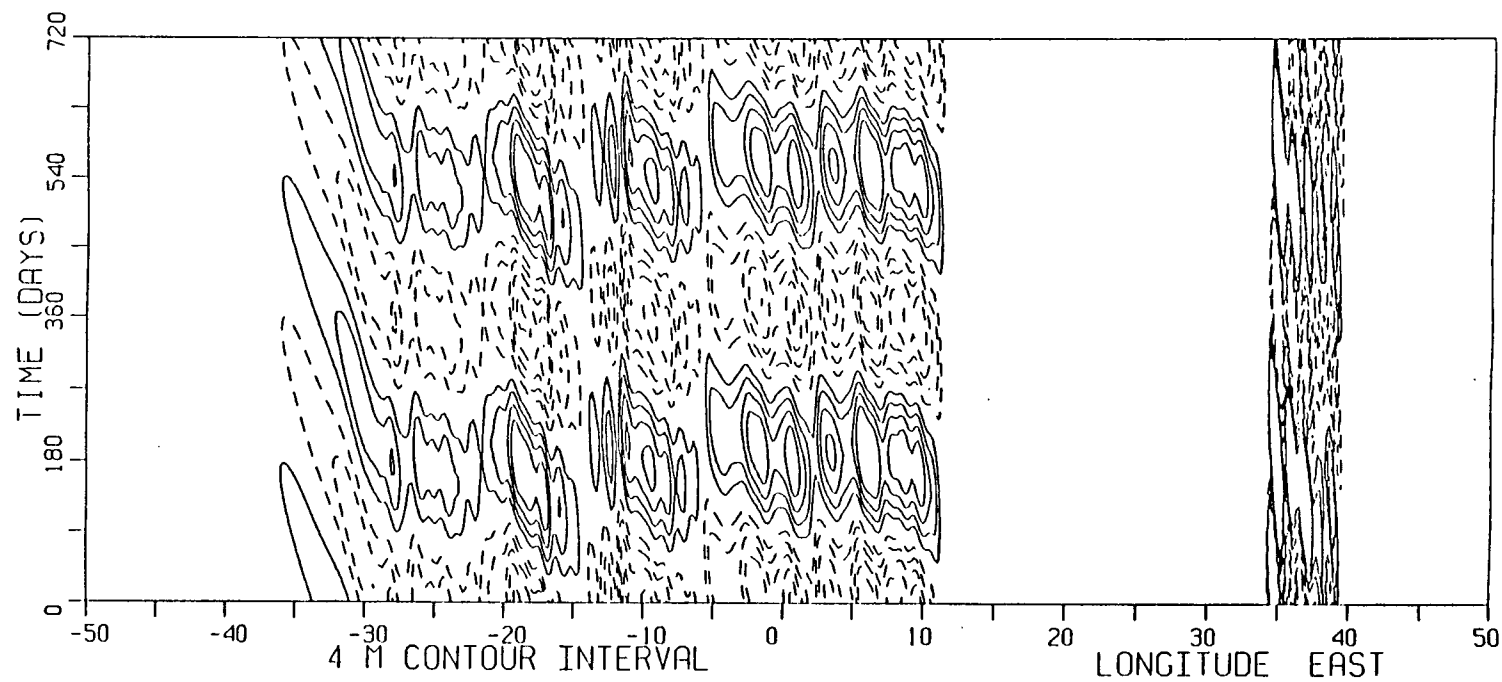
Figure 8b. Longitude-time plot of the thermocline height field along 31 S.

Indian Ocean including a large area to the south east of Madagascar (Cheney et al, 1983). Since there are indications of meanders and eddies in the Agulhas Current (Harris et al, 1978) in the Mozambique Channel and south west of Madagascar it is likely that it is these features rather than the short Rossby waves which cause the observed variability.

Longitude-time plots :

Although all the longitude-time plots (Figures 8a.-f.) show the general westward propagation of phase required for a Rossby wave, by looking at the relative spacing between the contours one can get an idea of the horizontal wavelength of the waves in different parts of the domain. This information is now considered in light of the above discussion. It is clear that at any given latitude the waves in the Indian Ocean are much shorter than those in the South Atlantic. As far as the latter are concerned, far from the Southern African coast (say west of the Greenwich meridian) there appears to be a trend towards smaller wavelengths at higher latitudes (as Figure 4a. confirms). Also, the longer waves near the southwestern tip of Africa which have arisen from the Agulhas Bank wind source and the 'roaring forties' can be seen along 42 S and 45 S. Another feature, which is also confirmed by Figure 4a. is the relatively quiet area for waves in the region 42 S to 45 S,5 W to 2 E.

Wavenumber vectors of the Rossby wave field :

Through analysis of the latitude-time and longitude-time plots, it has been possible to match the wave sets to the various sources by determining the general direction of energy and phase propagation. However, in order to determine these directions more accurately, it is necessary to compute the wavenumber vectors.

The points in the model domain where one is interested in calculating these vectors is on the paths in the wave field along which the wave energy is propagated, i.e. in the direction of the group velocity of the waves. It is appropriate to use ray theory to determine these paths (Longuet-Higgins, 1964) as, by definition, wave rays are the characteristic curves of the wave equation in space and are tangential to the group velocity. In general, ray theory is valid as long as no rays intersect or overlap (i.e. there should be no caustic surfaces in the wave field). But prior to this stage, if the wave amplitude begins to vary significantly
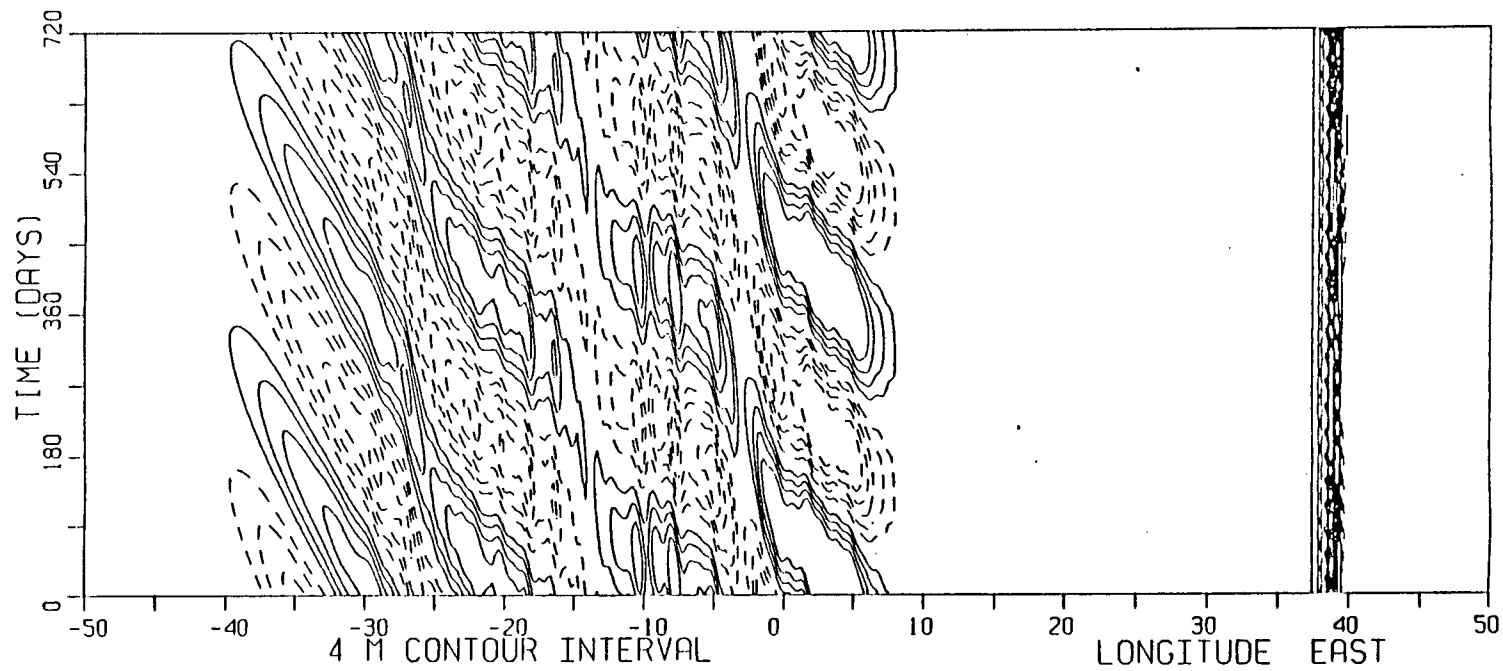
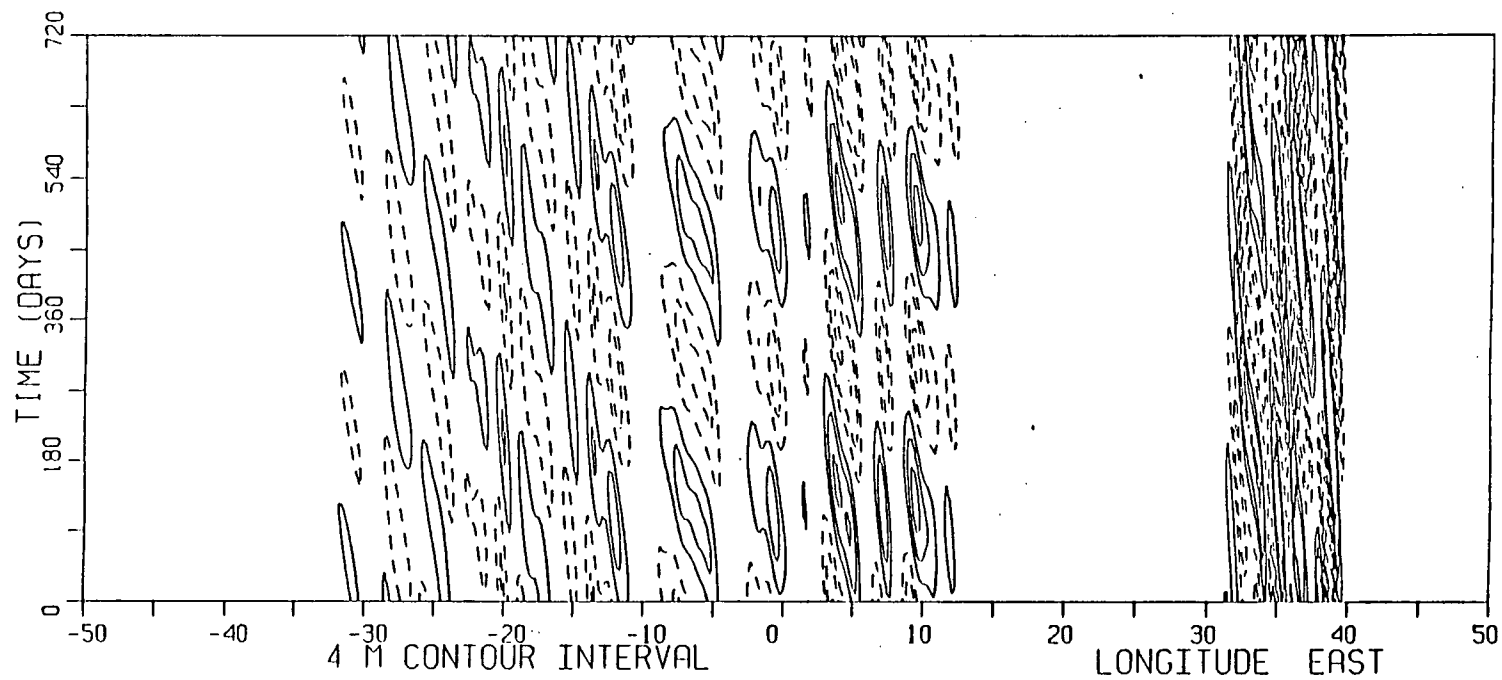Figure 8c. Longitude-time plot of the thermocline height field along 25 S.

Figure 8d. Longitude-time plot of the thermocline height field along 35 S.
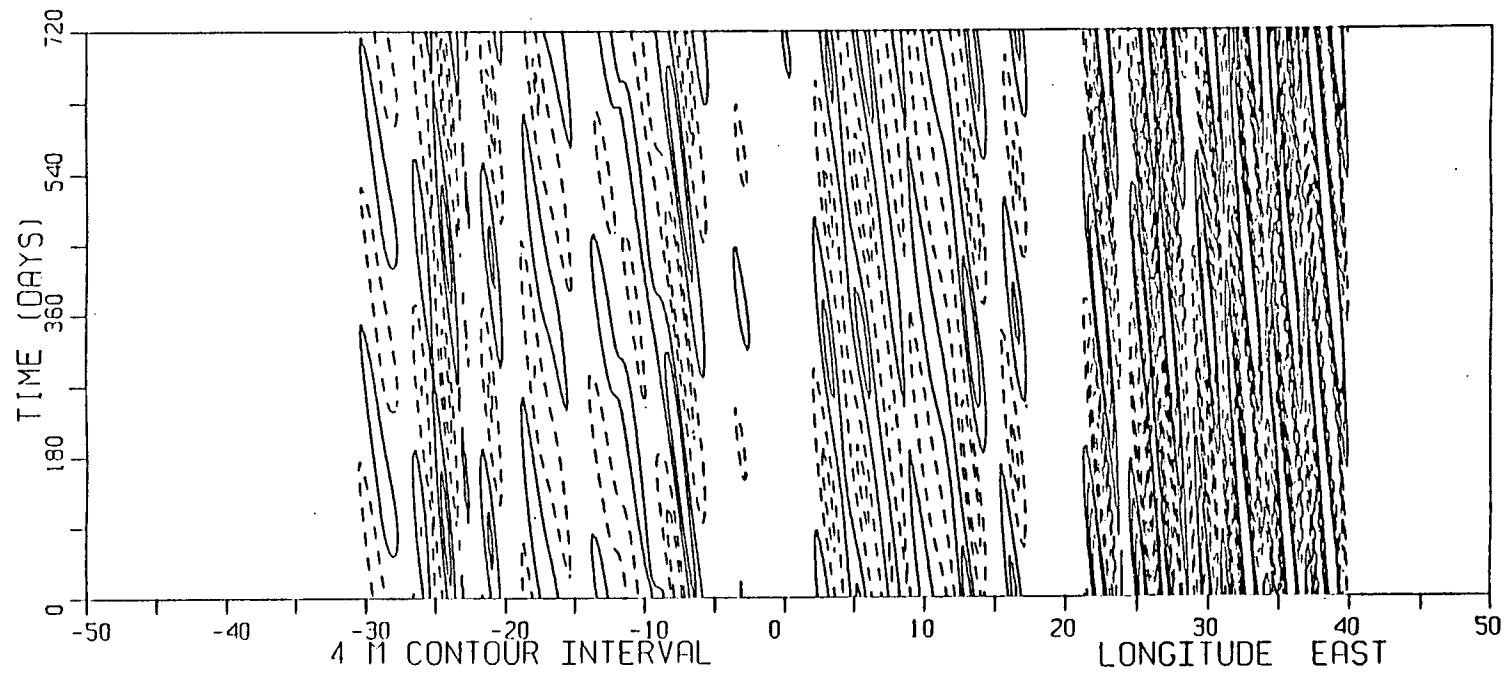
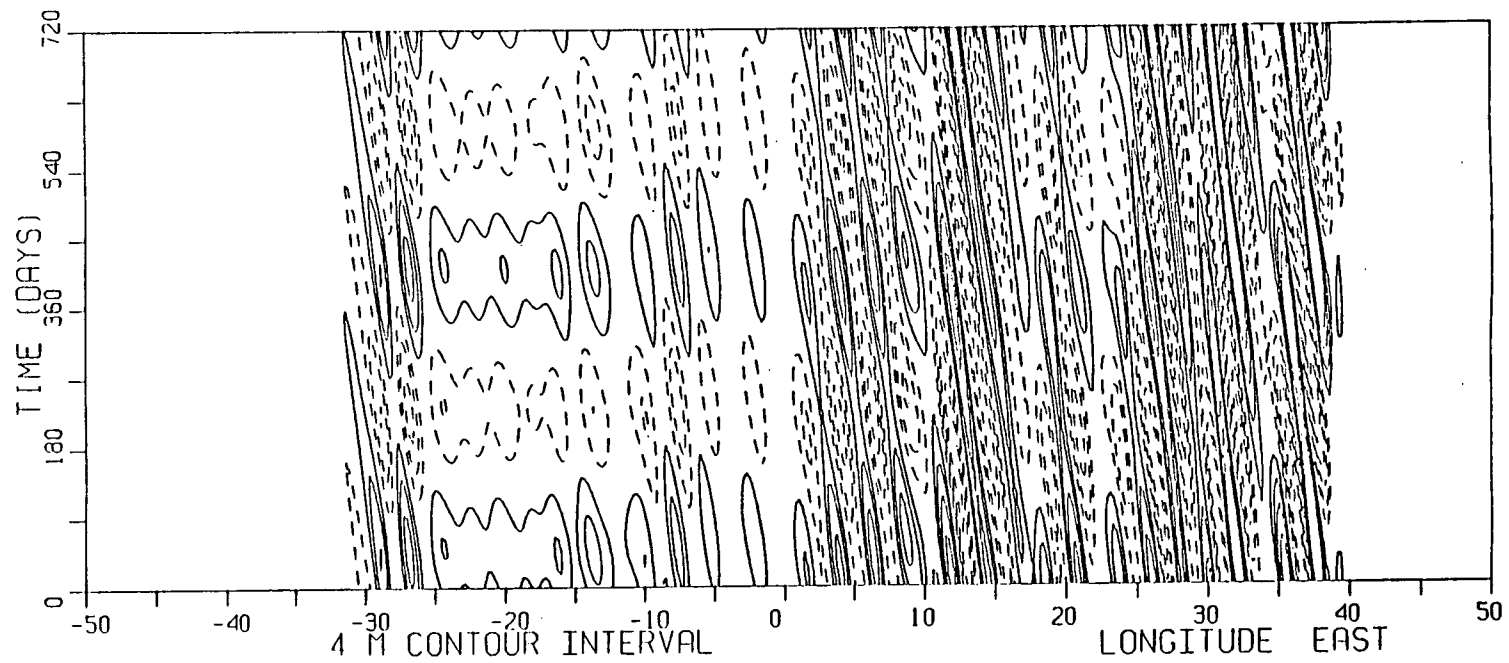Figure 8e. Longitude-time plot of the thermocline height field along 42 S.

Figure 8f. Longitude-time plot of the thermocline height field along 45 S.

over a wavelength or period of the wave then the approximation deteriorates. It should also be mentioned that the slowness circle theory discussed above tacitly assumes that ray theory holds local to the wave disturbance.

A sufficiently accurate and by far the simplest way of obtaining the wave rays from the model field is to draw a curve through coherent patterns of adjacent maxima of crests and troughs in Figure 4a.-c. while bearing in mind the phase information contained in the longitude and latitude-time plots.

Having fixed the points where the vectors are to be evaluated one then needs to determine the amplitude and phase of the annual harmonic in the model thermocline anomaly data. This is performed in exactly the same manner as for the wind field so that the thermocline displacement is written as

$$h(\lambda, \theta) = H(\lambda, \theta)cos(\omega t + \Phi(\lambda, \theta))$$

where H is the amplitude and $\Phi$ is the phase.

According to Cummins et al (1986), the wavenumber vector $\underline{k}(\lambda, \theta)$ can then be defined as

$$\underline{k} = \nabla \Phi$$

where $\nabla$ is the gradient operator in spherical co-ordinates.

Once the harmonic analysis program has computed the phase $\Phi$, the gradient is calculated using the standard finite difference approximation at the selected points. Figure 9 shows the vectors for 5 different rays in the South Atlantic Ocean; namely those originating near 23 S,11 E; 24 S,11 E; 32 S,11 E; 30 S,21 W and 40 S,18 E. For future reference the rays are labelled A to E respectively. Note that the scale of 1.5 units in Figure 9 corresponds to a wavenumber magnitude of $1.5 \times 10^{-5} m^{-1}$ (i.e. a wavelength of 420 km).

In general the results are consistent with the slowness circle arguments given above. For example, on rays A and B near 20 S the phase can be seen to become more poleward in direction as the wave rays and energy refract equatorward. Similarly, the general southwest propagation of phase all along the 40 S latitude and the change in phase between 30 S and 34 S, 21 W to 29 W (corresponding to the mid ocean wave source) is evident. Since the
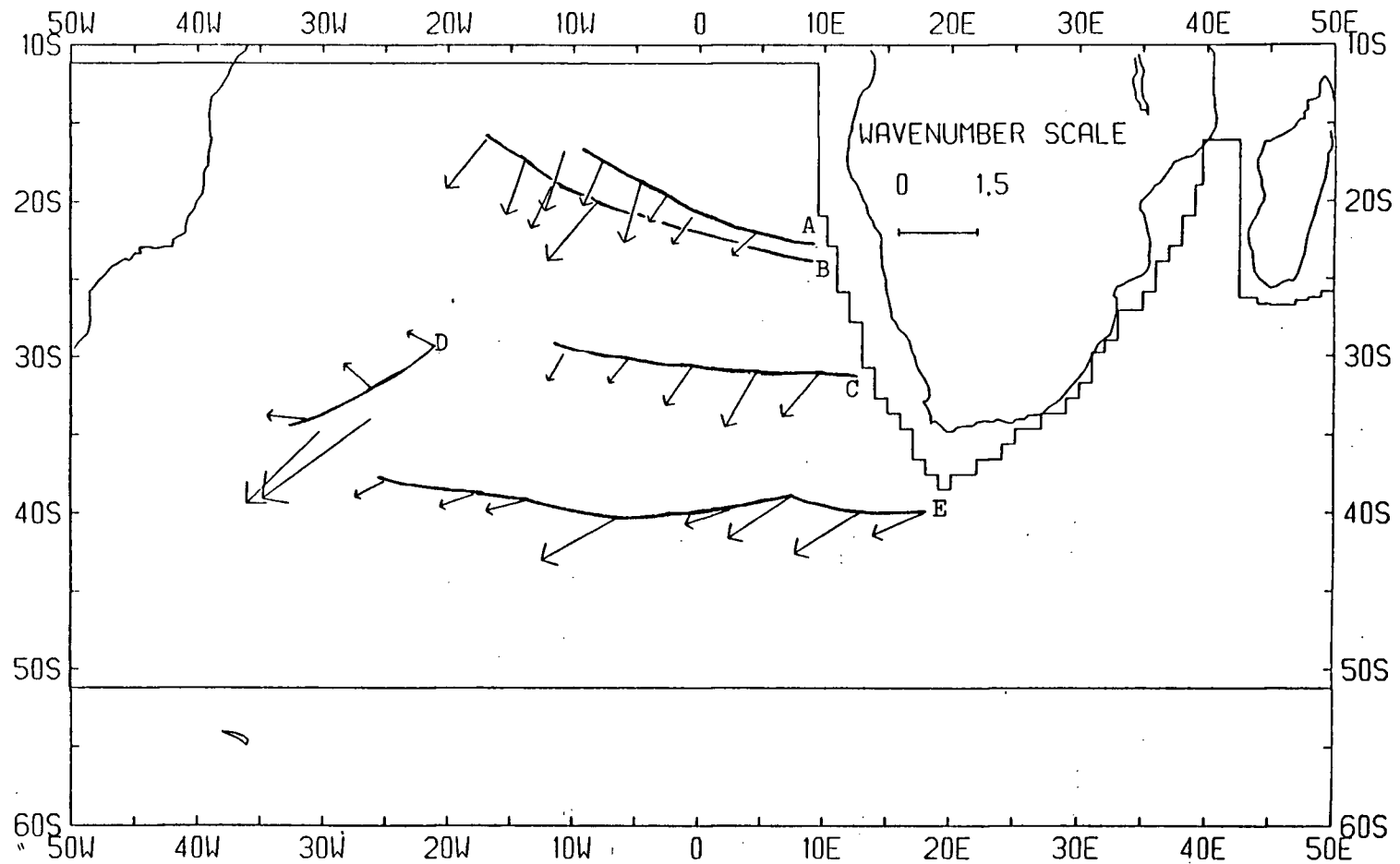
# Rossby Wavenumbers

Figure 9. Wavenumber vectors computed at points along wave rays near 20 S, 32 S, 35 S and 40 S. Units of wavenumber magnitude are $10^{-5}m^{-1}$.

magnitude of the wavenumber vectors determine the wavelength as $2\pi|k|^{-1}$ the following estimates for wave sets in different parts of the model domain can be made.

For rays A and B, wavelengths range from 900 km at 23 S,5 E to 400 - 500 km around 18 S,12 W with associated phase speeds of $2.9cm\ s^{-1}$ and $1.3$ to $1.6cm\ s^{-1}$. Along ray C the wavelengths and phase speeds are about 560 km and $1.8cm\ s^{-1}$ near the coast, 1050 km and $3.3cm\ s^{-1}$ at 30.1 S,5 W. Between 25 S and 35 S, 15 W and 30 W there is a pronounced wave train arising from the mid ocean wave source with wavelengths and phase speeds of 240 - 480 km and $0.8cm\ s^{-1}$ to $1.5cm\ s^{-1}$, respectively. Note that for the sake of clarity, Figure 9 shows only two wavenumber vectors from this train. These are located at 34 S,26 W and 35 S,30 W. Further north, along ray D longer and faster waves (1000 km and $3.2cm\ s^{-1}$), which have arisen from the Namibian coast, are evident. Finally, along ray E (39 S to 40 S band), the waves increase in length and speed from about 400 km and $1.3cm\ s^{-1}$ near 20 E to 900 km and $2.9cm\ s^{-1}$ near 15 W.

Although the zonal component of the wavenumber vector should be conserved as the waves refract (Schopf et al, 1981), Figure 9 shows that this is not always the case. Possible reasons explaining this inconsistency include inaccuracies in determining the exact ray path traced out by the wave disturbances and the existence of inhomogeneities at certain points in the wave field due to local Ekman pumping and the generally complex structure of the wave field. Also, variations in the slope of the coastline in several places and the likelihood of ray paths from different sources intersecting each other present difficulties.

Geostrophic velocities:

By means of the geostrophic relations it is possible to calculate the particle velocities associated with the annual harmonic in the thermocline displacement. The velocities are expressed as root mean square values with respect to the annual period. It should be noted that using the geostrophic relations assumes that the waves are propagating freely i.e., the calculations are only valid for those areas in the model domain where the wind forcing is relatively small.

Referring to Figure 10, a contoured plot of the velocities, it is clear that the contours
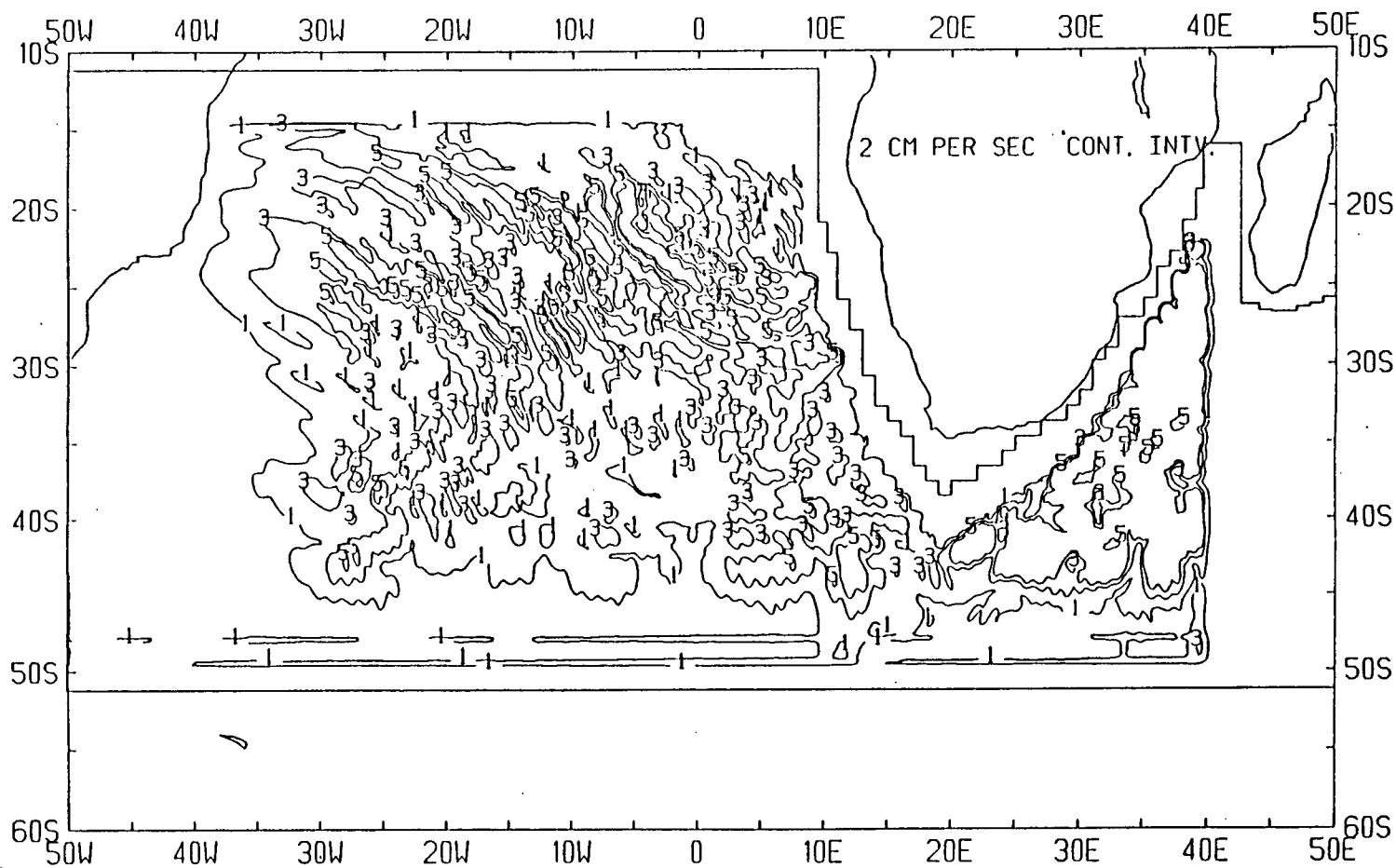
# RMS Velocity Contours



Figure 10. Root mean square geostrophic velocities of magnitude 5 *cm* $s^{-1}$ or less associated with the Rossby wave field.
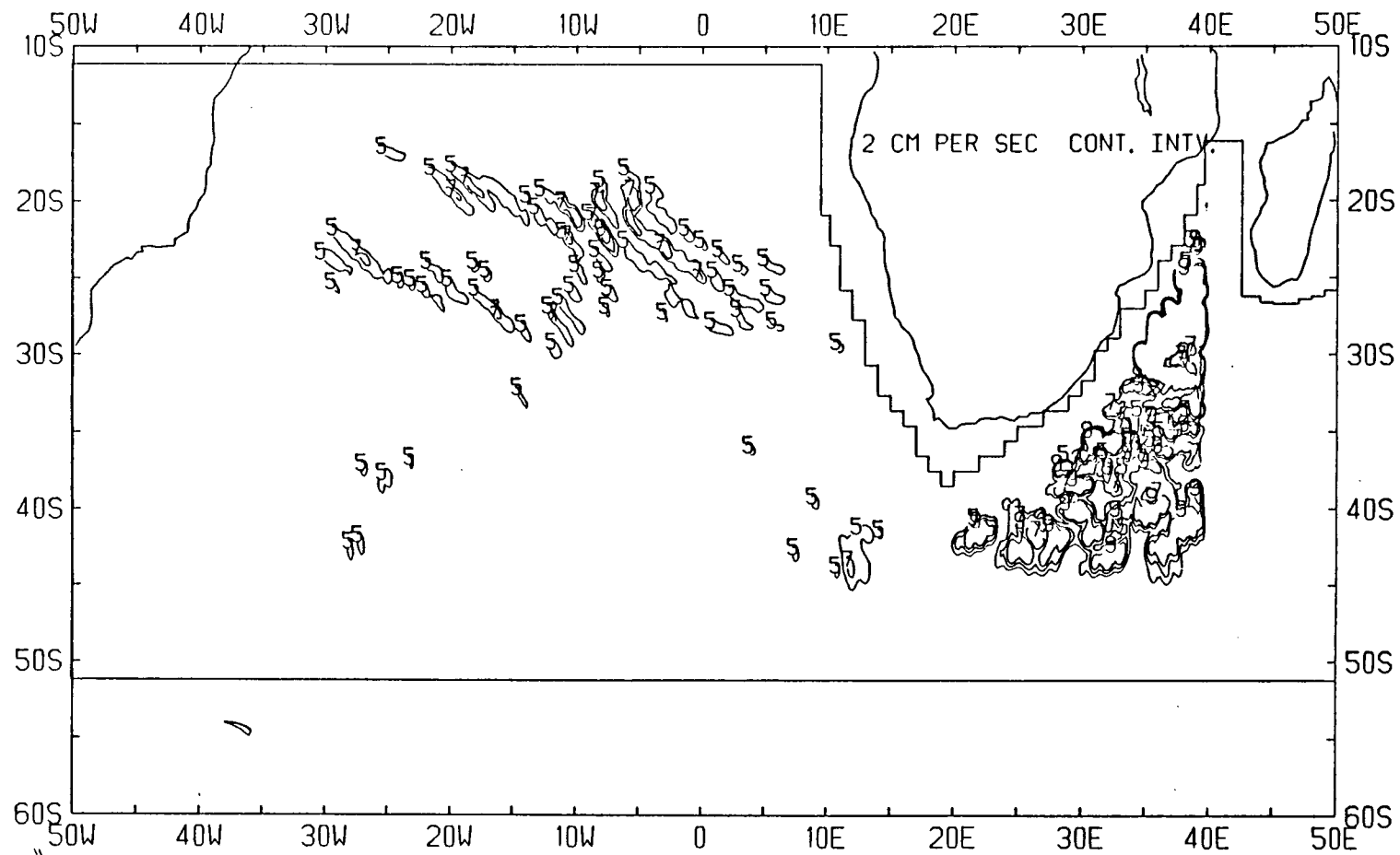
# RMS Velocity Contours



Figure 11. Root mean square geostrophic velocities of magnitude 5 *cm* $s^{-1}$ or more associated with the Rossby wave field.

are roughly aligned with the wavecrests of the thermocline distribution. This result is consistent with the waves being transverse. Note that for the sake of clarity, Figure 10 only plots values less than $5 cm\ s^{-1}$ whereas Figure 11 shows the areas in the domain where the velocities are $5 cm\ s^{-1}$ or greater. In general, the rms currents are strongest where the wavelengths of the waves are small and the pressure gradients largest.

For example, near the critical latitude and sponge layers where the wave motion is dying out, the currents are very small. On the other hand, for the waves emanating from the Namibian coast they are large, reaching a maximum of $7 - 8 cm\ s^{-1}$ in the region 18 S to 28 S,0 W to 30 W. There is also an area of strong currents in the coastal ocean off the South Western Cape near 44 S,11 E. Note that the very large model currents in the South West Indian Ocean are excluded from the discussion due to doubts about the ability of the model grid to resolve the short waves there.

Since these values are of the same order or even larger than the phase velocities of the waves it would seem that the nonlinear advective terms, which have been neglected in the model equation (2.2), might be of importance. However, it is known (see Kang and Magaard, 1980) that for a monochromatic field of plane Rossby waves the nonlinear terms exactly cancel. Since the thermocline distribution in Fig.4a. shows the model field to consist largely of plane or nearly plane waves, neglect of these terms is unlikely to be important.

Figure 12 shows a sample instantaneous current field computed from the thermocline distribution contoured in Figure 4a. Note that only the vectors in the South Atlantic have been plotted. The results are generally consistent with the above remarks. One point of added interest is that it is possible at a few points (e.g. the Namibian coast near 27 S,5 E) to trace out the anticlockwise direction of the current vectors which correspond to a high pressure or raised thermocline. The reverse is true for a thermocline depression.
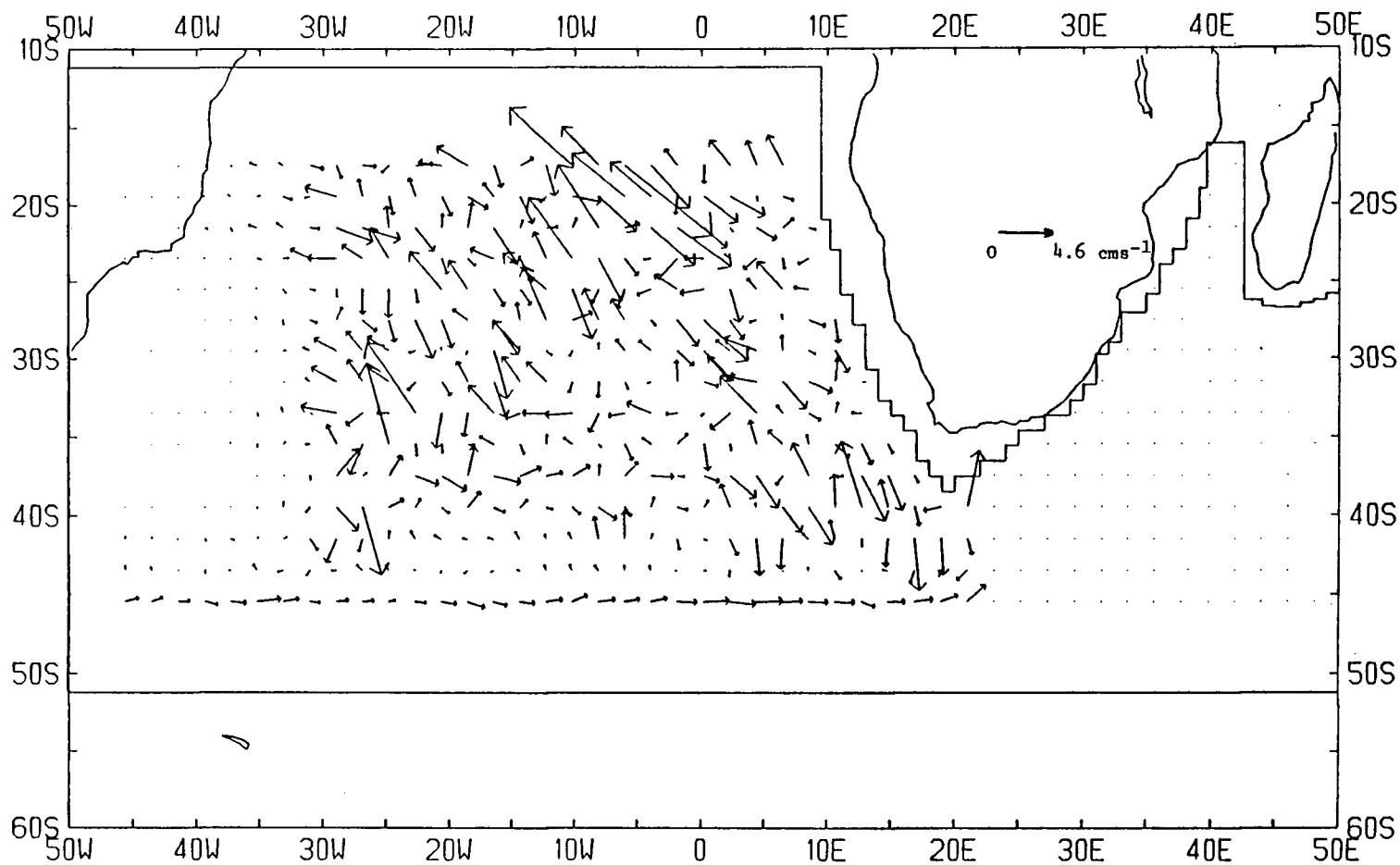
# Velocity vectors



Figure 12. Instantaneous geostrophic velocities associated with the thermocline height field shown in Figure 4a. Scaling : a 1 cm long vector corresponds to a velocity of 4.6 *cm s⁻¹*.

# 6.Conclusion

The model has been able to demonstrate that, similar to the North Pacific, westward propagating Rossby waves are efficiently generated in the South Atlantic Ocean by a seasonally varying wind stress curl. This wind stress curl field is of complex structure with several localised maxima which are potential wave sources. From the phase information available in the latitude-time and longitude-time plots at various sections in the model field and by application of the slowness curve theory for free Rossby waves it has been possible to identify the probable wind source for each train of waves.

A summary of these wave sources is as follows :

1. Namibian coastal source near 25 S,10 E : The strong winds here reach a maximum curl of at least $30 \times 10^{-9} dyne\ cm^{-3}$ and generate waves with energy propagating northwest towards the equator between 23 S and 15 S but poleward between 25 S and 29 S.

2. Agulhas Bank source near 38 S,25 E : Maximum wind stress curls here are $(15 - 19) \times 10^{-9} dyne\ cm^{-3}$ and waves are propagated with energy both in the westward and northwestward direction in the South Atlantic between 30 S and 38 S,25 E to 2 E. There is also wave energy propagation eastward into the South Indian Ocean between 31 S and 46 S.

3. Mid ocean source near 38 S,10 W : Peak wind stress curls reach $(25 - 29) \times 10^{-9} dyne\ cm^{-3}$ with associated equatorward propagation of wave energy between 15 S and 36 S but zonal propagation along the 37 S - 39 S band.

4. 'Roaring forties' wave source between 46 S and 51 S at all longitudes but especially near 10 W and 2 E : Wind intensities range from $(10 - 40) \times 10^{-9} dyne\ cm^{-3}$. Wave energy is propagated basically westward but with a small northward component between 47 S and 41 S near 10 W and 2 E.

5. Natal/Mozambique coastal source along 23 S to 31 S, 35 E : In this area, winds vary over $(15 - 24) \times 10^{-9} dyne\ cm^{-3}$. Short Rossby waves with southeastward propagating energy are generated.

Apart from efficient wave generation, the model is also able to demonstrate wave

properties like refraction and reflection. Refractive behaviour of the waves can be exhibited by the model field because the model equations include a Rossby radius that varies with latitude, as in the real ocean. In agreement with the theory of Schopf et al (1981), the model wave energy is refracted towards the equator. There is in general a transport of this energy northwards in the model wave field which could have implications for the modelling of annual fluctuations in the water properties of the equatorial South Atlantic Ocean.

Another important feature of the study is that by including the relative vorticity term in the model equations, waves are able to propagate in other than a strictly zonal direction. Earlier models by White (1977) and White and Saur (1981) for example, neglected this term so that only purely westward propagating waves were obtained.

Comparing the model wave field presented here to that obtained by using the same basic model in the North Pacific (Cummins et al ,1986) shows that the wave field in the South Atlantic is somewhat more complex in its structure. This result is consistent with the greater number of potential wave sources (i.e. more maxima in the wind field) present in this region as well as the greater variation in the continental boundaries. Examples of the latter include the termination of Africa as a continent in mid ocean at 35 S, which allows waves generated by the winds near the Agulhas Bank to propagate into the South Atlantic Ocean and which also causes reflection and short wave propagation off its eastern coast, and the narrower expanse of ocean between Africa and South America compared to the breadth of the North Pacific Ocean.

Both the refraction and reflection properties of the Rossby waves were explained in a heuristic manner by slowness curve theory. This theory assumed that the waves are freely propagating and plane and that wave rays along which the wave energy is transported to be readily identifiable in the model wave field. Once the waves have left their areas of generation and encounter no further vorticity sources this is indeed a reasonable approximation. Subsequent calculations of the wavenumber vectors and the root mean square geostrophic velocities associated with the waves were in general agreement with the slowness curve analysis.

The main focus of the study was directed towards Rossby wave generation and propagation in the South Atlantic Ocean, although the existence of short Rossby waves in the model South West Indian Ocean was also clearly demonstrated. Analysis of this area could only be qualitative since the model grid is too coarse to resolve the short waves here to any great degree of accuracy. In addition the Agulhas Current, a strong western boundary current of this ocean, would need to be included in any realistic study of the area. This would be a formidable task, due to the general meandering and eddy shedding behaviour of the Agulhas, and would perhaps be of limited application as field observations of Rossby waves under these conditions is, to say the least, unlikely.

Even restricting the detailed wave analysis to the South Atlantic Ocean does not rule out consideration of the Agulhas Current entirely, because as discussed in the introductory section of this thesis, eddies have been observed to shed from the retroflection region of this current and then to propagate around into the south east corner of the South Atlantic Ocean. It is also interesting to note that the location of the retroflection region itself fluctuates on long time scales (months to years) so that it is possible that Rossby waves may be generated in this way. However, by far the largest part of the South Atlantic is relatively quiet in terms of eddy activity (Cheney et al, 1983) with similar levels of mesoscale variability and dynamics to the central North Pacific (Thomson, 1986) where Rossby waves have been observed.

Other non-linear effects neglected in our model include interaction with a mean current. Killworth (1979) has shown that refraction of wave energy from mean currents can be important if these currents have a substantial zonal component. Thus, the Benguela Current which flows northwards along the west coast of Southern Africa is unlikely to be of importance in this regard but the westward flowing South Equatorial Current which extends as far as 15 S or so may well be.

Finally, the possibility of vertical mixing of wave energy and the inclusion of a continuously stratified ocean would also need to be considered in a more sophisticated model. As far as the latter is concerned, one would expect the waves generated by the wind stress

curl in a continuously stratified ocean to be of smaller amplitude than those obtained here in our reduced gravity model where the wind acts as a body force in the upper layer.

Nevertheless, after bearing all these considerations in mind, it is felt that the linear model described here has demonstrated conclusively that Rossby waves can be generated by a seasonally varying wind stress curl in the South Atlantic Ocean. Slowness curve analysis and wavenumber computations have shown that the model waves are reflected and refracted in the expected manner so it now remains for field studies to be conducted. Hopefully these would be able to confirm the existence of Rossby waves in this part of the world ocean and would identify the length and time scales involved. All that can be mentioned at this stage is that our long wave scales in the South Atlantic and short scales in the South West Indian Ocean are consistent with the scales detected in the depths of the $\sigma_t = 26.2$ and salinity surfaces observed by Lutjeharms (1981b). Also, the inferred direction of flow obtained from measurements made during a hydrographic survey off the Cape of Good Hope, Gruendlingh and Lutjeharms (1979), is consistent with the direction of our model Rossby wave field there. To conclude, it may be said that Rossby wave generation and propagation in the South Atlantic Ocean is probable on the basis of this theoretical study and by comparison with the energy levels in the North Pacific Ocean (where these waves have been observed), but the question cannot be definitely settled until field observations have been conducted. One promising possibility is the upcoming IOS (U.K.)/ONR (U.S.) Southern Oceans cruise, planned for 1987 which will take CTD measurements along transects between 30 S and 50 S, 5 W and 25 E (Pollard 1986).

# References

Boudra,D.B., and W.P.M. de Ruijter,1986: The wind driven circulation of the South Atlantic-Indian Ocean. II: Experiments using a multi-layer numerical model. *Deep Sea Research* , in press.

Bunker,A.F.,1976: Computations of surface energy flux and annual air-sea interaction cycles of the North Atlantic Ocean. *Monthly Weather Review*, 104, 1122–1140.

Camerlengo,A.L., and J.J.O'Brien,1980: Open boundary conditions in rotating fluids. *Journal of Computational Physics*, 35, 12–35.

Cane,M.A., and E.S.Sarachik,1981: The response of a linear baroclinic ocean to periodic forcing. *Journal of Marine Research* , 39, 651–693.

Cheney,R.E., J.G.Marsh, and B.D.Beckley,1983: Global mesoscale variability from collinear tracks of SEASAT altimeter data. *Journal of Geophysical Research* , 88, 4343–4354.

Cummins,P.F., L.A.Mysak and K.Hamilton,1986: Generation of annual Rossby waves in the North Pacific by the wind stress curl. *Journal of Physical Oceanography*, 16, 1165–1178.

de Ruijter,W.P.M.,1982: Asymptotic analysis of the Agulhas and Brazil Current systems. *Journal of Physical Oceanography*, 12, 361–373.

de Ruijter,W.P.M., and D.B.Boudra,1985: The wind driven circulation in the South Atlantic-Indian Ocean. I: Numerical experiments in a one layer model. *Deep Sea Research* , 32, 557–574.

Duncan,C.P.,1965: An eddy in the subtropical convergence southwest of South Africa. *Journal of Geophysical Research* , 73, 531–534.

Emery,W.J., and L.Magaard,1976: Baroclinic Rossby waves as inferred from temperature fluctuations in the Eastern Pacific. *Journal of Marine Research* , 34, 365–385.

Emery,W.J., W.Lee, and L.Magaard,1984: Geographic and seasonal distributions of Brunt-Vaissala frequency and Rossby radii in the North Pacific and North Atlantic. *Journal of Physical Oceanography,* 14, 294–317.

Foreman,M.G.G.,1977: Manual for tidal heights analysis and prediction. *Pacific Marine Science Report,* 7710. Institute of Ocean Sciences, Patricia Bay, B.C.

Gill,A.E.,1982: Atmosphere-Ocean Dynamics. Academic Press, 662 pp.

Gordon,A.L.,1985: Indian-Atlantic transfer of thermocline water at the Agulhas Retroflection. *Science,* 227, 1030- -1033.

Gruendlingh,M.L.,1983: Eddies in the Southern Indian Ocean and the Agulhas Current. In:*Eddies in Marine Science,* Robinson,A.R. ,(ed.). Springer-Verlag, 609 pp.

Gruendlingh,M.L., and J.Lutjeharms,1979: Large-scale flow patterns of the Agulhas Current System. *South African Journal of Science*, 75, 269- -270.

Haidvogel,D.B., and P.B.Rhines,1983: Waves and circulation driven by oscillatory winds in an idealized ocean basin. *Geophysical and Astrophysical Fluid Dynamics*, 25, 1–63.

Harris,T.F.W.,R.Legeckis and D.van Foreest,1978: Satellite IR images in the Agulhas Current. *Deep Sea Research* , 25, 543–548.

Hellerman,S., and M.Rosenstein,1983: Normal monthly wind stress over the world ocean with error estimates. *Journal of Physical Oceanography,*13, 1093– 1104.

Kamstra,F.,1985: Environmental features of the Southern Benguela with special reference to the wind stress. In: *South African Ocean Colour and Upwelling Experiment.*, Shannon,L.V., (ed.). Sea Fisheries Research Institute, Cape Town ,270pp.

Kang,Y.Q., and L.Magaard,1980: Annual baroclinic Rossby waves in the central North Pacific. *Journal of Physical Oceanography*, 10, 1159–1167.

Killworth,P.D.,1979: On the propagation of stable baroclinic Rossby waves through a mean shear flow. *Deep Sea Research* , 26, 997–1032.

Krauss,W., and C.Wuebber,1982: Response of the North Atlantic to annual wind variations along the eastern coast. *Deep Sea Research* , 29, 851–864.

LeBlond,P.H., and L.A.Mysak,1978: Waves in the Ocean. Elsevier, 602 pp.

Longuet-Higgins,M.S.,1964: On group velocity and energy flux in planetary wave motions. *Deep Sea Research* , 11, 35–42.

Lutjeharms,J.,1981b: Spatial scales and intensities of circulation in ocean areas adjacent to South Africa. *Deep Sea Research* , 28, 1289–1302.

Lutjeharms,J., and H.R.Valentine,1984: Southern Ocean thermal fronts south of Africa. *Deep Sea Research* , 31, 1461-1475.

Lutjeharms,J., and R.C.van Ballegooyen,1984: Topographic control in the Agulhas Current system. *Deep Sea Research* , 31, 1321- 1337.

Magaard,L.,1977: On the generation of baroclinic Rossby waves in the ocean by meteorological forces. *Journal of Physical Oceanography*, 7, 359–364.

McCreary,J.P.,1976: Eastern tropical ocean response to changing wind systems: with application to El Niño. *Journal of Physical Oceanography*, 6, 632–645.

McCreary,J.P., S.R.Shetye and P.K.Kunda,1986: Thermohaline forcing of eastern boundary currents: With application to the circulation off the west coast of Australia. *Journal of Marine Research* , 44, 71–92.

Moore,D., and S.G.H.Philander,1976: Modelling of the equatorial oceanic circulation. In:*The Sea*, Vol.6, Goldberg,E.D., I.N. McCave, J.J.O'Brien, and J.H.Steele (Eds.), 1047 pp.

Mysak,L.A.,1983: Generation of annual Rossby waves in the North Pacific. *Journal of Physical Oceanography*, 13, 1908–1923.

Nelson,C.S.,1977: Windstress and wind stress curl over the California Current. NOAA Tech. Rep. NMFS-SSRF-714, August, 1977.

Olson,D.B., and R.H.Evans,1986: Rings of the Agulhas Current. *Deep Sea Research* , 33, 27–42.

Ou,H.W., and W.P.M. de Ruijter,1985: Separation of an inertial boundary current from a curved coastline. *Journal of Physical Oceanography*, 16, 280–289.

Pedlosky,J.,1979: Geophysical Fluid Dynamics. Springer-Verlag, 624 pp.

Pollard,R.T.,1986: Southern Oceans 1987. *pers.comm.*

Price,J.M., and L.Magaard,1983: Rossby wave analysis of subsurface temperature fluctuations along the Honolulu-San Francisco great circle. *Journal of Physical Oceanography*, 13, 258–268.

Raymond,W.H., and H.L.Kou,1984: A radiation boundary condition for multi-dimensional flows. *Quarterly Journal of the Royal Meteorological Society*, 110, 535– 551.

Schopf,P.S., D.L.T.Anderson, and R.Smith,1981: Beta-dispersion of low-frequency Rossby waves. *Dynamics of Atmospheres and Oceans*, 5, 187–214 .

Shannon,L.V. (Ed.),1985: South African Ocean Colour and Upwelling Experiment. Sea Fisheries Research Institute, Cape Town, 270pp.

Thomson,K.A.,1986: On the geographic variability of oceanic mesoscale motions. Ph.D. Thesis, Department of Oceanography, University of British Columbia, Vancouver, B.C.

van Foreest,D., F.A.Shillington, and R.Legeckis,1984: Large scale, stationary, frontal features in the Benguela current system. *Continental Shelf Research*, 3, 465–474.

van Loon,H., and J.C.Rogers,1984a: Interannual variations in the half-yearly cycle of pressure gradients and zonal wind at sea level on the southern hemisphere. *Tellus*, 36A, 76-86.

van Loon,H., and J.C.Rogers,1984b: The yearly wave in pressure and zonal geostrophic wind at sea level on the southern hemisphere and its interannual variability. *Tellus*, 36A, 348–354.

Wajsowicz,R.C.,1986: Free planetary waves in finite difference numerical models. *Journal of Physical Oceanography*, 16, 773–789.

White,W.B.,1977: Annual forcing of baroclinic long waves in the tropical North Pacific. *Journal of Physical Oceanography*, 8, 818–824.

White,W.B., and J.F.T.Saur,1981: A source of annual baroclinic waves in the eastern subtropical North Pacific. *Journal of Physical Oceanography*, 11, 1452–1462.

White,W.B., and J.F.T.Saur,1983: Sources of interannual baroclinic waves in the eastern subtropical North Pacific. *Journal of Physical Oceanography* , 13, 531–544.

Willmott,A.,1985: The generation of baroclinic Rossby waves by meridional oscillations of a zonal wind stress. *Geophysical and Astrophysical Fluid Dynamics*, 34, 39–63.

# Appendix

The Rossby wave equation :

The purpose of this section is to give a brief description of how one can derive the Rossby wave equation (2.2) used in the model.

As a starting point we consider the governing equations for motion in the upper layer of a two-layer ocean with the lower layer assumed to be at rest. In their linearised form on a beta plane these equations take the form

$$u_t - fv + g'h_x = \frac{\tau^x}{\rho_o H_o} - r_o u, \qquad (A.1)$$

$$v_t + fu + g'h_y = \frac{\tau^y}{\rho_o H_o} - r_o v, \qquad (A.2)$$

$$h_t + H_o(u_x + v_y) = -r_o h, \qquad (A.3)$$

where u and v are velocity components in the x and y directions, h is the interfacial displacement (positive downwards), $\tau^x$ and $\tau^y$ are the eastward and northward components of the wind stress, $\rho_o$ and $H_o$ are the density and unperturbed depth of the upper layer, $g'$ is the reduced gravity and f is the Coriolis parameter. For a beta plane $f = 2\Omega \sin\theta$ is approximated by $f = f_o + \beta y$ where $f_o = 2\Omega \sin\theta_o$ , $\beta = 2\Omega \cos\theta_o / a$ , $\Omega$ is the earth's rotation rate, a is its radius and $\theta$ is the latitude ($\theta_o$ is a given fixed latitude at the centre of the beta plane).

In order to arrive at the Rossby wave equation (2.2), a single equation for the thermocline displacement h is derived from equations (A.1) to (A.3) and then scaling arguments appropriate to quasi-geostrophic motions in a rotating two-layer ocean are introduced. Thus the length L and velocity U scales are assumed to be such that the Rossby number Ro = U/fL and the sphericity parameter $\beta^* = \beta L/f_o$ are both much less than unity. Quasigeostrophy also requires that the Burger number $B = (R/L)^2$, where R is the internal Rossby radius to be defined below, be of order unity but since we have assumed a reduced gravity ocean this assumption is not needed here. As the physical justification for invoking quasi-geostrophy has already been discussed in Section 2, it will suffice here to say

that the term quasi-geostrophy arises from the fact that the horizontal component of the long period (e.g. Rossby wave time scale) motions in a rotating fluid for which $Ro \ll 1$ are nearly in geostrophic balance i.e.

$$f\underline{k} \times \underline{u} = -\frac{1}{\rho}\nabla p$$

where p is the pressure and $\rho$ is the density.

To derive a single equation for h one can proceed as follows. Equation (A.2) multiplied by f is added to equation (A.1) operated on by $(\partial_t + r_o)$ and similarly equation (A.1) multiplied by f is added to the operated version of (A.2). Then u and v are eliminated by using equation (A.3). Restricting the possible dynamics to Rossby waves is achieved by making the low frequency assumption $|(\partial_t + r_o)h| \ll |fh|$ and by assuming the x and y scales to be comparable. After neglecting terms $g'^2\beta h_{yt}f^{-3}$ and $\underline{\tau} \times \nabla(f^{-1})$, on the basis of the quasigeostrophic scales, in comparison to $-g'\beta h_x f^2$ and $f^{-1}curl_z\underline{\tau}$ respectively, we arrive at

$$(\frac{\partial}{\partial t} + r_o)(\nabla^2 - R^{-2})h + \beta^* h_x = \frac{curl_z\underline{\tau}}{\rho_o R^2 f}, \qquad (A.4)$$

where R is the Rossby deformation radius and is the natural length scale of the problem. It is defined as

$$R = \frac{\sqrt{g'H_o}}{f}$$

Equation (A.4) is the Cartesian beta plane form of equation (2.2). The spherical polar form of (A.4) (i.e. equation (2.2)) can be derived from the spherical polar forms of (A.1) to (A.3) using the method outlined above. However for the purpose of determining the basic properties of the waves and the dispersion relation we simply deal with the unforced, frictionless form of (A.4), i.e.,

$$\frac{\partial}{\partial t}(\nabla^2 - R^{-2})h + \beta^* h_x = 0, \qquad (A.5)$$

In order to obtain the dispersion relation for free, unattenuated waves we substitute the nearly plane wave solution for a beta plane i.e.

$$h(x, y, t) = A(x, y)e^{i(kx + ly - \omega t)}$$

into the Rossby wave equation (A.5) to obtain

$$\omega = \frac{-\beta k}{(k^2 + l^2 + R^{-2})},$$
(A.6)

where k and l are the x and y wavenumbers respectively. Equation (A.6) is the dispersion relation for free Rossby waves of the first baroclinic mode in a beta plane ocean. These waves arise through the variation of the Coriolis parameter with latitude (the so called beta effect) as from equation (A.5) it can be seen that it is the $\beta^* h_x$ term which acts as the restoring term for the wave motions.

From the definition $\underline{c}_p = \frac{\omega}{k^2} \underline{k}$ the phase velocity is determined by the dispersion relation as

$$\underline{c}_p = \frac{1}{(k^2 + l^2)(k^2 + l^2 + R^{-2})}(-\beta k^2, -\beta kl),$$
(A.7)

Hence the phase velocity always has a $-k$ component which means that the phase of the Rossby wave must always propagate in a generally westward direction. A useful manner in which to represent the dispersion relation is via the slowness curve; this is simply the curve of constant $\omega$ in $\underline{k}$ space.

Rearranging (A.6) yields the slowness curve

$$(k + \frac{\beta}{2\omega})^2 + l^2 = \frac{\beta^2}{4\omega^2} - R^{-2},$$
(A.8)

a circle of radius

$$\sqrt{(\frac{\beta}{2\omega})^2 - R^{-2}}$$

and centre

$$(k, l) = (-\frac{\beta}{2\omega}, 0)$$

It follows from equation (A.8) that for the right hand side to be positive, we must have $\omega^2 < (\beta/2f)^2 g'H_o$. After substituting the definitions $f = 2\Omega sin\phi_o$ and $\beta = 2\Omega cos\phi_o/a$ we obtain the inequality

$$tan\phi_o < \frac{\sqrt{g'H_o}}{2a\omega}$$

i.e. no Rossby waves of a fixed frequency can propagate beyond the critical latitude $tan^{-1}\sqrt{g'H_o}/2a\omega$ . For the parameters used in the model, namely, $g' = 1.5 \times 10^{-2} ms^{-2}, H_o = 500m, a = 6371km$ and $\omega = 1.997 \times 10^{-7} s^{-1}$ (the annual frequency) the critical latitude is 47.2 S.

Since the group velocity vector $c_{gi}$ is given by the wavenumber gradient of the dispersion relation $\omega(k_i)$; i.e. $c_{gi} = \frac{\partial \omega}{\partial k_i}$ it is perpendicular in direction to the slowness curve $\omega = constant$ in the direction of increasing $\omega$ and so must be directed along a straight line from the circumference of the circle to its centre. Taking the gradient of (A.6) yields

$$\underline{c}_g = \frac{\beta}{(k^2 + l^2 + R^{-2})^2}(k^2 - l^2 - R^{-2}, 2kl), \tag{A.9}$$

Hence, in general $\underline{c}_g$ is neither parallel nor perpendicular to the phase velocity. In fact for a given frequency and phase direction $\theta$ there are generally two Rossby waves which may propagate, a short wave and a long wave, a result which is most easily appreciated by substituting the polar co-ordinate representation for the horizontal wavenumber into

the slowness equation (A.8) i.e. substitute $k = k_h cos\theta, l = k_h sin\theta$ where $k_h^2 = k^2 + l^2$ and $cos\theta < 0$. Expanding and solving for $k_h$ yields

$$k_h^s = \frac{-\beta}{2\omega}cos\theta + \sqrt{\frac{\beta^2}{4\omega^2}cos^2\theta - R^{-2}}$$, the short wave with associated group velocity $\underline{c}_{gs}$

and

$$k_h^l = \frac{-\beta}{2\omega}cos\theta - \sqrt{\frac{\beta^2}{4\omega^2}cos^2\theta - R^{-2}}$$, the long wave with associated group velocity $\underline{c}_{gl}$.

Figure 13 illustrates the situation in terms of the slowness diagram. For any given direction of phase propagation $\theta$, which must always have a $-k$ or westward component, the short Rossby wave with phase velocity $\underline{c}_p^s$ and group velocity $\underline{c}_g^s$ and long wave of phase velocity $\underline{c}_p^l$ and group velocity $\underline{c}_g^l$ are as shown. A limiting case occurs when $\theta$ is such that the phase velocity vector is just tangent to the slowness curve. Then $k_h^s = k_h^l$ and the two group velocities are identical. On the other hand, if $\theta = 180^o$ then the two group velocities have the same magnitude but are opposite in direction; $\underline{c}_g^l$ being directed westward but $\underline{c}_g^s$ is eastward, the phase velocities are westward as usual. This special case is of particular interest in our model for that part of the ocean to the south and east of the Southern African landmass where both refraction and reflection of Rossby waves off the western boundary into the ocean is evident. It has been discussed in detail in Section 5. Another interesting property of the slowness circle, which is also dealt with in that section, is that due to the variation of the Rossby radius with latitude, the radius tends to increase as one moves towards the equator and decrease nearer the pole. As a consequence, long Rossby waves that are zonal in direction have greater velocities nearer the equator.

The fact that the group and phase velocities of a Rossby wave are usually in different directions illustrates the anisotropic nature of these waves. Due to this property the
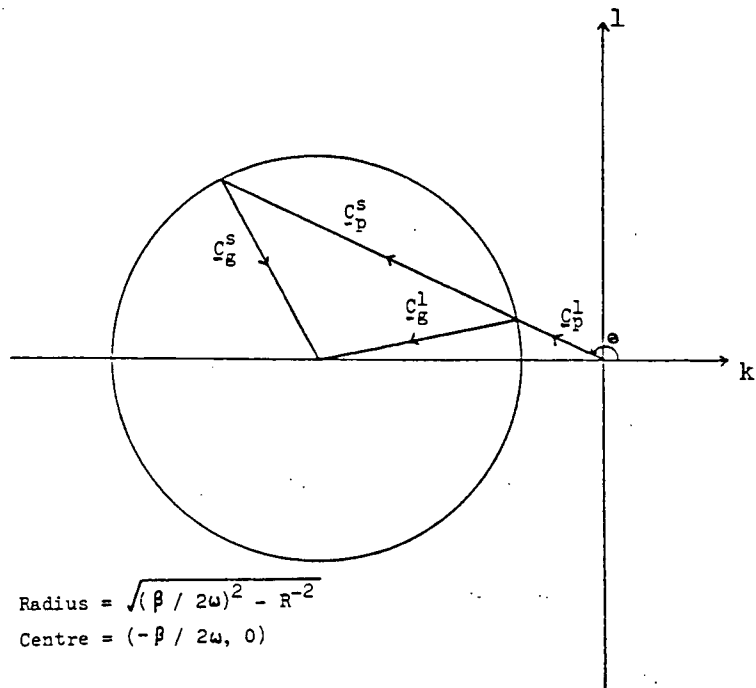
Figure 13. Slowness curve representation of the dispersion relation for free Rossby waves.

analysis of wave characteristics like reflection and refraction of wave energy is usually not as straightforward as they are for isotropic wave types. However it is possible by making the carrier wave transformation

$$h(x, y, t) = \psi(x, y)e^{-i(\frac{\beta x}{2\omega} + \omega t)}$$

to derive a Helmholtz type equation which is satisfied by isotropic wave motions (see LeBlond and Mysak, 1978 for details). This results in a slowness curve in the $(k', l)$ plane, where $k' = k + \frac{\beta}{2\omega}$ , of radius $\sqrt{(\frac{\beta}{2\omega})^2 - R^{-2}}$ and centre the origin. Then for any given direction of phase propagation $(k', l)$ there is only one Rossby wave that can propagate. It has its group velocity in the opposite direction to the phase i.e. towards the origin of the $(k', l)$ plane and so may make complex wave reflection problems easier to handle.

Damping Layers :

Apart from its usefulness for determining how the model Rossby waves propagate the dispersion relation (A.6) can also be employed as a guide for designing the damping layers required by the model. To do so one needs to include the Rayleigh damping coefficient in the Rossby wave equation and hence in the dispersion relation. The result (see Mysak, 1983) is

$$\omega = -\frac{\beta k}{(k^2 + l^2 + R^{-2})} - ir_0, \qquad (A.10)$$

As already discussed in Section 2, the purpose of these damping regions is to prevent spurious reflection of wave energy back into the model domain. Such reflections can occur both at the edge of the damping layer (if the damping there is too strong) or within the layer itself. Additionally, it must be ensured that the waves are sufficiently attenuated by the Rayleigh dissipation coefficient $r_o$. In general, the best way of satisfying these criteria

is to impose a wide layer with a large value of $r_o$ at the boundary of the model domain which gradually merges into the frictionless and non-diffusive interior of the model domain where $r_o = 0$.

From equation (A.10) it can be seen that if $r_o > 0$ then the Rossby waves will decay exponentially with time scale $T_d = 1/r_o$. Hence for the damping layer to attenuate the waves efficiently $T_d$ should be much greater than the time scale associated with the propagation of wave energy into the layer, $T_w$. Since the energy of wave motions is always propagated at the group velocity, $T_w$ can be approximated by $\frac{\Delta x}{c_g}$ where $\Delta x$ is the spacing of the model grid and $c_g$ is the group velocity normal to the damping layer. Hence $c_g$ is given by the relevant component of equation (A.9) depending on whether the damping is along the vertical or horizontal wall of the domain. Note that its magnitude depends on both the latitude and the direction of propagation of the wave.

As an example consider a zonally travelling ( $l = 0$ ) Rossby wave incident on the western sponge layer which extends from 46 W to 26 W. Substituting in typical values of the parameters into equation (A.9) shows that $c_{gx}$ and hence $T_w^{-1}$ decrease approximately exponentially with increasing latitude. To account for this behaviour, the western damping region, in addition to its decline in strength across its width, has an exponential taper of $r_0$ with latitude with an e-folding scale of some 750km. Hence the ratio $T_d/T_w$ for these waves is of the order of 50-100 at any given latitude and this means that there will be a gradual attenuation of the incoming wave energy through the layer. As is evident from the plots of the thermocline anomaly this form of damping layer results in no significant reflection of wave energy off the model boundaries.

Damping was also imposed on the eastern and northern boundaries. The eastern layer, whose purpose is to attenuate the waves emanating off the nearby southeast coast of Africa, is of a similar form to the western layer. However, it is ten rather than twenty degrees in width. Attenuation of these waves is particularly severe since their eastward group velocity is only a tenth or so of that of the westward group velocity of the waves propagating into the western sponge layer. Due to the small area of ocean between the

east coast of Southern Africa and the eastern boundary of the model this strong damping is justified. On the other hand, the damping in the northern layer is somewhat weaker than the western region because the northward component of the waves is much less than the westward component. Figure 14 illustrates the variation of $r_o$ across the western layer at 15 S (labelled B) and across the northern layer (labelled A). As mentioned above, the eastern damping region is of the same form as the western except that it is only ten degrees in extent.
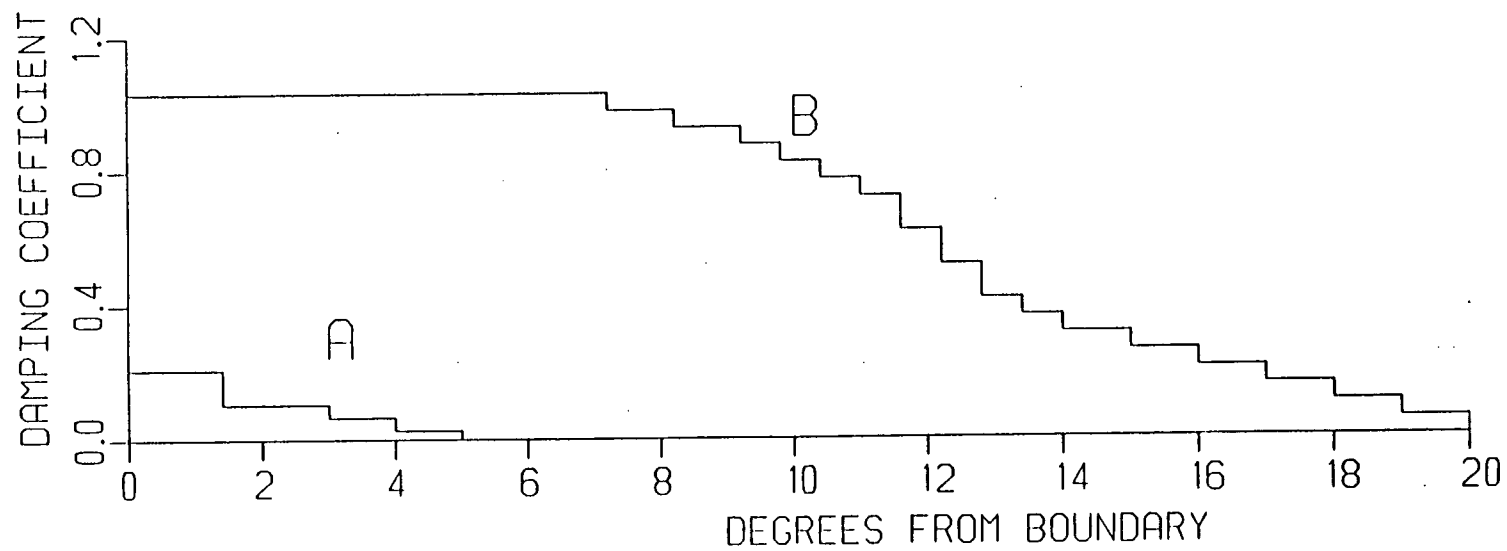
Figure 14. The form of the damping layers imposed along the northern, western and eastern boundaries of the model domain.